

**Hydrogen isotope  
modelling**

G. Pieterse et al.

# Global modelling of H<sub>2</sub> mixing ratios and isotopic compositions with the TM5 model

**G. Pieterse<sup>1</sup>, M. C. Krol<sup>1,2</sup>, A. M. Batenburg<sup>1</sup>, L. P. Steele<sup>3</sup>, P. B. Krummel<sup>3</sup>,  
R. L. Langenfelds<sup>3</sup>, and T. Röckmann<sup>1</sup>**

<sup>1</sup>Institute for Marine and Atmospheric Research Utrecht (IMAU), Utrecht, The Netherlands

<sup>2</sup>Department of Meteorology and Air Quality at Wageningen University, Wageningen, The Netherlands

<sup>3</sup>Centre for Australian Weather and Climate Research, CSIRO Marine and Atmospheric Research, Australia

Received: 1 December 2010 – Accepted: 2 February 2011 – Published: 17 February 2011

Correspondence to: T. Röckmann (t.roeckmann@uu.nl)

Published by Copernicus Publications on behalf of the European Geosciences Union.

Title Page

Abstract

Introduction

Conclusions

References

Tables

Figures

◀

▶

◀

▶

Back

Close

Full Screen / Esc

Printer-friendly Version

Interactive Discussion



## Abstract

The isotopic composition of molecular hydrogen ( $H_2$ ) contains independent information for constraining the global  $H_2$  budget. To explore this, we have implemented hydrogen sources and sinks, including their isotopic composition, into the global chemistry transport model TM5. For the first time, a global model now includes a simplified but explicit isotope reaction scheme for the photochemical production of  $H_2$ . We present a comparison of modelled results for the  $H_2$  mixing ratio and isotope composition with available measurements on the seasonal to inter annual time scales for the years 2001–2007. The base model results agree well with observations for  $H_2$  mixing ratios. For  $\delta D[H_2]$ , modelled values are slightly lower than measurements. A detailed sensitivity study is performed to identify the most important parameters for modelling the isotopic composition of  $H_2$ . The results show that on the global scale, the discrepancy between model and measurements can be closed by adjusting the default values of the isotope effects in deposition, photochemistry and the stratosphere-troposphere exchange within the known range of uncertainty. However, the available isotope data do not provide sufficient information to uniquely constrain the global isotope budget. Therefore, additional studies focussing on the isotopic composition near the tropopause and on the isotope effects in the photochemistry and deposition are recommended.

## 1 Introduction

The role of molecular hydrogen ( $H_2$ ) as a possible energy carrier is an ongoing subject of debate in the political as well as the academic arena. In contrast to fossil fuels, which produce the long-lived greenhouse gas carbon dioxide ( $CO_2$ ) and other undesired compounds (e.g. carbon monoxide, nitrogen oxides and soot) upon oxidation with oxygen ( $O_2$ ),  $H_2$  only produces water ( $H_2O$ ). Hence, using  $H_2$  instead of fossil fuels could improve air quality and reduce the human impact on global climate. Unlike fossil fuels,  $H_2$  is not available in large reservoirs, and the above mentioned positive effect can only be

ACPD

11, 5811–5866, 2011

## Hydrogen isotope modelling

G. Pieterse et al.

Title Page

Abstract

Introduction

Conclusions

References

Tables

Figures

◀

▶

◀

▶

Back

Close

Full Screen / Esc

Printer-friendly Version

Interactive Discussion



achieved if H<sub>2</sub> is produced from carbon-free resources.

In previous studies, potential adverse effects of the introduction of a hydrogen fuel economy were also identified. These effects are all related to the notion that a hydrogen fuel economy would lead to enhanced atmospheric mixing ratios of H<sub>2</sub> due to leakage in the production, distribution, storage and use of H<sub>2</sub>. H<sub>2</sub> is an important reaction partner of the hydroxyl radical (OH). Therefore, higher H<sub>2</sub> mixing ratios would consume OH radicals that would otherwise be available for the removal of other trace gases (Schultz et al., 2003), e.g. the greenhouse gas methane (CH<sub>4</sub>). Other studies investigated an adverse effect on the recovery of the ozone hole (Tromp et al., 2003; Warwick et al., 2004; Feck et al., 2008). Higher stratospheric H<sub>2</sub> mixing ratios lead to higher levels of stratospheric water vapour, which can result in increased formation of polar stratospheric clouds that would enhance polar ozone destruction.

The global H<sub>2</sub> cycle has been investigated by numerous studies, (e.g., Seiler and Conrad, 1987; Warneck, 1988; Ehhalt, 1999; Novelli et al., 1999; Hauglustaine and Ehhalt, 2002; Sanderson et al., 2003; Price et al., 2007) and the present state of knowledge has been recently reviewed by Ehhalt and Rohrer (2009), see Table 2 in Sect. 3.4. H<sub>2</sub> is produced by the atmospheric oxidation of methane (CH<sub>4</sub>) and non methane hydrocarbons (NMHCs). Direct surface sources are from fossil fuel burning, biomass burning, and nitrogen fixation in the terrestrial biosphere and the oceans. H<sub>2</sub> is removed by atmospheric oxidation and by dry deposition. Current estimates for the chemical lifetime of H<sub>2</sub> vary between 1.4 and 2.3 years, and for the total atmospheric burden between 141 and 172 Tg H<sub>2</sub>. However, the uncertainties in the magnitudes of the different sources and sinks are even larger and call for further research.

Following the approach introduced by Gerst and Quay (2001), isotope measurements have been used to obtain further constraints on the individual source and sink strengths. The isotopic composition of methane-derived H<sub>2</sub> was investigated by measurements in the stratosphere (Rahn et al., 2003; Röckmann et al., 2003; Rhee et al., 2006, 2008) as well as by detailed laboratory studies (Feilberg et al., 2004, 2005, 2007a,b; Rhee et al., 2008; Nilsson et al., 2007; Röckmann et al., 2010; Nilsson et al.,

**Hydrogen isotope  
modelling**

G. Pieterse et al.

Title Page

Abstract

Introduction

Conclusions

References

Tables

Figures

◀

▶

◀

▶

Back

Close

Full Screen / Esc

Printer-friendly Version

Interactive Discussion



2009). Isotope signatures for the surface sources are based on few early studies by Gerst and Quay (2001), and Rahn et al. (2002a,b, 2003). More detailed studies have been published very recently (Vollmer et al., 2010; Röckmann et al., 2010). Price et al. (2007) were the first to implement the isotope signatures for H<sub>2</sub> sources and sinks in a full global chemistry transport model. The actual isotope chemistry involved with the oxidation of CH<sub>4</sub> and the NMHCs was not implemented but the resulting isotopic  $\delta D[H_2]$  signature of the photochemical source of H<sub>2</sub> was optimised to a value of +162<sup>+57</sup><sub>-57</sub>‰ to close the isotope budget. In this work, the values for  $\delta D[H_2]$  are calculated from the ratio  $R = D/H$  as  $\delta D[H_2] = (R/R_{VSMOW} - 1)$ , where  $R_{VSMOW} = 1.558 \times 10^{-4}$  is the reference D/H ratio of Vienna Standard Mean Ocean Water. How this isotopic composition progresses through the CH<sub>4</sub> and NMHC oxidation chain, however, is still an open question.

In a recent study, Pieterse et al. (2009) derived and evaluated a hydrogen isotope chemistry scheme including the full methane oxidation chain and a condensed NMHC oxidation scheme. The findings of the experimental studies by Feilberg et al. (2004, 2005, 2007a,b); Nilsson et al. (2007, 2009) and Rhee et al. (2008) were incorporated into the resulting model framework. The result was a chemistry scheme that is internally consistent with respect to the derived kinetic isotope effects (KIEs), and the isotopic branching (IB) ratios. This work describes the implementation of this new isotope chemistry scheme in version 5 of the global Transport Model (TM5) developed by Krol et al. (2005), summarised in Sect. 2. In contrast to previous studies, this implementation allows for a detailed analysis of the full H<sub>2</sub> cycle, including its stable isotopologue HD because the isotopic composition of the intermediate compounds and the enrichment due to the oxidation of CH<sub>4</sub> and the NMHCs are explicitly calculated. Furthermore, the sensitivity of the isotopic composition to changes in the initial isotopic composition of CH<sub>4</sub> and the NMHCs, or to changes in the isotope kinetics in each reaction of the photochemical pathway from CH<sub>4</sub> to H<sub>2</sub> can be calculated. With the implementation of the explicit isotope scheme in TM5, the global budgets of H<sub>2</sub> and HD can be fully assessed.

**Hydrogen isotope  
modelling**

G. Pieterse et al.

Title Page

Abstract

Introduction

Conclusions

References

Tables

Figures

◀

▶

◀

▶

Back

Close

Full Screen / Esc

Printer-friendly Version

Interactive Discussion



**Hydrogen isotope  
modelling**

G. Pieterse et al.

[Title Page](#)[Abstract](#)[Introduction](#)[Conclusions](#)[References](#)[Tables](#)[Figures](#)[◀](#)[▶](#)[◀](#)[▶](#)[Back](#)[Close](#)[Full Screen / Esc](#)[Printer-friendly Version](#)[Interactive Discussion](#)

In Sect. 3, the modelled H<sub>2</sub> mixing ratios are compared with available measurements from the National Oceanic and Atmospheric Administration (NOAA), reported in Novelli et al. (1999), the Australian Commonwealth Scientific and Research Organisation (CSIRO), and the Advanced Global Atmospheric Gases Experiment (AGAGE), both reported in Xiao et al. (2007). Measurements provided by Rice et al. (2010) and the Eurohydros project (Batenburg et al., 2011) are used to evaluate the modelled isotopic composition of H<sub>2</sub>. After the experimental evaluation, the spatial vertical and surface patterns of the H<sub>2</sub> mixing ratio and isotopic composition are analysed. Finally, the global H<sub>2</sub> isotope budget and its sensitivity to changes in the parameters of the main processes, e.g. deposition, photochemistry, and the stratosphere-troposphere exchange (STE) are investigated. The overall conclusions are summarised in Sect. 4.

## 2 Model adaptations

### 2.1 Implementing condensed methane isotope chemistry

The chemistry in the TM5 model (Krol et al., 2005) is described by the Carbon Bond Mechanism 4 (CBM-4) introduced by Houweling et al. (1998). We have added the hydrogen isotope scheme described by Pieterse et al. (2009), thus extending the original CBM-4 reaction scheme by the important intermediate singly deuterated isotopologues (CH<sub>2</sub>DOO, CH<sub>2</sub>DOOH, CHDO, and HD). This will allow us to investigate for the first time the individual contributions of the individual reaction steps in the methane and NMHC oxidation chains to the final overall isotopic signature of the photochemical source of H<sub>2</sub> in the troposphere. The detailed derivation and implementation of the CH<sub>4</sub> reaction scheme is provided in Appendix A.

### 2.2 Implementing NMHC isotope chemistry

The non methane hydrocarbon (NMHC) chemistry was also adopted from CBM-4, and the photochemical NMHC chemistry scheme was extended with the singly deuterated

## Hydrogen isotope modelling

G. Pieterse et al.

[Title Page](#)[Abstract](#)[Introduction](#)[Conclusions](#)[References](#)[Tables](#)[Figures](#)[◀](#)[▶](#)[◀](#)[▶](#)[Back](#)[Close](#)[Full Screen / Esc](#)[Printer-friendly Version](#)[Interactive Discussion](#)

hydrogen isotope chemistry described by Pieterse et al. (2009), further described in Appendix B. A serious shortcoming for H<sub>2</sub> isotope modelling is that almost no information is available about the isotopic composition of the atmospheric NMHCs. The NMHC measurements themselves are difficult and in many cases just being developed and therefore almost no systematic atmospheric investigations exist. For the present study, we have chosen to deliberately set the isotopic composition of NMHCs to the average value for methane (−86‰), although in reality, the isotopic composition of these species might be lower. It would be useful to link the information available on bio synthesis of natural compounds from the field of biochemistry (e.g., Schmidt et al., 2003) to the atmosphere, but this is beyond the scope of this work. Because the atmospheric lifetime of most hydrocarbons is short, the singly deuterated companion species are not explicitly defined and transported in TM5. The reaction fluxes of the deuterated product species, such as deuterated formaldehyde, are calculated by correcting the fluxes of the non-deuterated product species using the above mentioned assumption for the initial isotopic composition. This means that for this initial study we also neglect the potential spatial and temporal variability of the isotopic composition of the NMHC species.

### 2.3 Parametrisation for the stratosphere

The TM5 model is primarily designed for modeling tropospheric chemistry, although a version focusing on stratospheric chemistry exists (van den Broek et al., 2003). Hence, the implementation of the stratospheric chemistry is rather crude and does not consider, for example, the oxidation of methane by chlorine radicals (Cl), and electronically excited oxygen atoms, O(<sup>1</sup>D). Therefore, we implemented an empirical linear parametrisation of HD relative to CH<sub>4</sub> as proposed by McCarthy et al. (2004) for the stratosphere. The following latitude ( $\theta$ ) dependent threshold pressure level  $p_s$  (Pa) separates the troposphere and the stratosphere:

$$p_s = 3.00 \times 10^4 - 2.15 \times 10^4 \cos(\theta). \quad (1)$$

## Hydrogen isotope modelling

G. Pieterse et al.

Title Page

Abstract

Introduction

Conclusions

References

Tables

Figures

◀

▶

◀

▶

Back

Close

Full Screen / Esc

Printer-friendly Version

Interactive Discussion



For all pressures below the threshold pressure level, the CBM-4 mixing ratios for H<sub>2</sub> and HD chemistry are replaced by the empirical parametrisation. Because H<sub>2</sub> and HD are transported as separate species, the TM5 model requires an explicit expression for the mixing ratio of both species as a function of CH<sub>4</sub>, which is derived from the results of McCarthy et al. (2004). The four-dimensional variational (4-D-Var) data assimilation system implemented in TM5 (Meirink et al., 2008a,b) was used to obtain the background CH<sub>4</sub> mixing ratios for the troposphere as well as the stratosphere. In order to constrain the H<sub>2</sub> mixing ratio and isotopic composition at the tropopause to 530 ppb and +130‰, the original HD-CH<sub>4</sub> relation was slightly modified (units in ppb):

$$[\text{HD}] = -6.32 \times 10^{-5}[\text{CH}_4] + 0.301. \quad (2)$$

For  $\delta\text{D}[\text{H}_2]\text{-CH}_4$ , the data presented in McCarthy et al. (2004) yield (units in ‰):

$$\delta\text{D}[\text{H}_2] = -0.267[\text{CH}_4] + 610. \quad (3)$$

These expressions fit the experimental data within the typical range of uncertainty of  $\pm 1\%$  for the H<sub>2</sub> mixing ratios, and  $\pm 10\%$  for the isotopic compositions. The stratospheric H<sub>2</sub> mixing ratio is then approximated by:

$$[\text{H}_2] = \frac{1}{2(\delta\text{D}[\text{H}_2] + 1)R_{\text{VSMOW}}}[\text{HD}]. \quad (4)$$

Here,  $R_{\text{VSMOW}} (= 1.558 \times 10^{-4})$  is the reference D/H ratio of Vienna Standard Mean Ocean Water. The factor 2 accounts for the fact that the isotopic composition is measured at a per atom basis, while there are two hydrogen atoms in the hydrogen molecule. Doubly deuterium substituted molecules are neglected in this study.

### 2.4 Implementing the surface sources

In the original implementation, TM5 uses the EDGAR3.2 inventory (Olivier and Berdowski, 2001) for the surface sources. The spatial distributions and relative magnitudes of the hydrogen surface emissions required for the calculations were obtained

**Hydrogen isotope  
modelling**

G. Pieterse et al.

Title Page

Abstract

Introduction

Conclusions

References

Tables

Figures

◀

▶

◀

▶

Back

Close

Full Screen / Esc

Printer-friendly Version

Interactive Discussion



from Schultz and Stein (2006). However, exploratory calculations with the original source magnitudes produced results that systematically underestimated the measured hydrogen mixing ratios. Therefore, we decided to scale the different source fluxes to the average of previously reported global budget estimates (Novelli et al., 1999; Hauglustaine and Ehhalt, 2002; Sanderson et al., 2003; Rhee et al., 2006; Price et al., 2007; Xiao et al., 2007; Ehhalt and Rohrer, 2009), resulting in the values shown in Tables 1 and 2 in Sect. 3.4. The upper and lower bounds of the averaged surface source magnitude estimates are also shown in the tables. The reported uncertainties in the individual papers are generally larger; up to  $\pm 10 \text{ Tg yr}^{-1}$  for the fossil fuel emissions and biomass burning, and up to  $\pm 5 \text{ Tg yr}^{-1}$  for  $\text{H}_2$  released from ocean and land  $\text{N}_2$  fixation. The isotopic signatures were adopted from Price et al. (2007).

## 2.5 Deposition parametrisation

The deposition scheme implemented in TM5, originally adopted from Ganzeveld et al. (1998) was extended for  $\text{H}_2$  and HD by implementing the surface resistance parametrisation for deposition of  $\text{H}_2$  reported by Conrad and Seiler (1980, 1985); Yonemura et al. (2000); Sanderson et al. (2003). In first tentative calculations with this scheme, the modelled  $\text{H}_2$  northern hemispheric mixing ratios were underestimated by about 10%. Decreasing the overall deposition velocity by the same amount resulted in the optimal agreement between the model and available data. This adaptation is justifiable because the corrected values are still well within the reported ranges of uncertainty (more than  $\pm 15\%$ ) for the underlying deposition measurements. The parametrisation includes seven ecosystem types, namely savanna, agricultural area, forests, grasslands/prairies, peat/tundra areas, semi-deserts, and deserts. These ecosystem types were assigned to the land use types defined by the European Centre for Medium-Range Weather Forecasts (ECMWF) that are implemented in the TM5 model.

The deposition scheme implemented in TM5 is an inferential deposition model (e.g., Garland, 1977; Hicks et al., 1991). The deposition flux  $F_C$  of a certain chemical species  $C$  to the surface is calculated as the difference between the ambient and surface mixing

ratio ( $[C]_a$  and  $[C]_0$ , respectively) multiplied with the deposition velocity of the chemical species,  $v_d$ :

$$F_C = -v_d([C]_a - [C]_0). \quad (5)$$

Generally,  $[C]_0$  is assumed zero so that only removal takes place. The overall resistance to deposition ( $R_t \equiv 1/v_d$ ) is the series resistance sum of i) the aerodynamic resistance ( $R_a$ ), which accounts for the turbulent diffusion in the surface layer, ii) the quasi-laminar boundary-layer resistance ( $R_b$ ), which accounts for the molecular diffusion through the layer just above the surface layer, and finally iii) the surface resistance ( $R_s$ ). Typically,  $R_s$  is the parallel resistance sum of the vegetation deposition resistance ( $R_{veg}$ ) and the soil deposition resistance ( $R_{soil}$ ), see for example Ganzeveld and Lelieveld (1995); Ganzeveld et al. (1998); Meyers et al. (1998). Technically, the chamber measurements performed by Gerst and Quay (2001) to determine the fractionation of the deposition process were conducted for conditions in which  $R_a \ll R_b + R_s$ . This implies that the fractionation constant should only be implemented for  $R_b$  and  $R_s$ . Moreover, turbulent diffusion, represented by  $R_a$ , will not introduce fractionation. However, in the majority of the field studies the total resistance is reported and therefore, we chose to implement an overall fractionation constant for the standard scenario calculations, i.e. the deposition velocity of HD was calculated by multiplying the resulting  $H_2$  deposition velocity with the overall fractionation constant of 0.943 for hydrogen deposition (Gerst and Quay, 2001).

### 3 Analysis of model results

#### 3.1 Comparison with $H_2$ mixing ratio measurements

Calculations were performed with a resolution of 6 by 4° (longitude-latitude) for the years 2001 to 2007 to ensure sufficient overlap with available measurements. Due to changes in the ECMWF native model, that is used to drive the atmospheric transport,

## Hydrogen isotope modelling

G. Pieterse et al.

Title Page

Abstract

Introduction

Conclusions

References

Tables

Figures

◀

▶

◀

▶

Back

Close

Full Screen / Esc

Printer-friendly Version

Interactive Discussion



the results for the years 2001–2005 were calculated using 25 vertical levels, whereas the results for 2006 and 2007 were obtained using 34 vertical levels. In this section, we compare the modelled  $H_2$  mixing ratio fields with available measurements.

Figure 1 shows the comparison of the model results for Alert (Canada) and the South Pole. For Alert, the seasonal signals are captured reasonably well, although deposition appears to be underestimated. The large variability (generally  $H_2$  depletion) in the measured mixing ratio at Alert is caused by soil uptake of  $H_2$  from the air masses arriving from the westerly direction due to deposition in the northern part of Russia during the northern hemispheric summer and autumn season. Such variability is absent at the South Pole because there is no ice-free land surface around the station. Note that the model assumes that there is no deposition to snow and ice. The figure shows good agreement for the stations at Barrow (Alaska) and Mace Head (Ireland). At the resolution used for the calculations, the model cannot capture the variability in the mixing ratios caused by local influences, but the seasonal cycles are adequately reproduced.

The measurements from Ascension Island (Atlantic Ocean) are characterised by little variability, as shown in Fig. 2. This station is hardly influenced by deposition and surface sources because it is situated far away from the major land masses. For Cape Grim (Tasmania), the model results show much more variability than the baseline values reported by NOAA and CSIRO. However, the comparison with the continuous AGAGE measurements shows that the unfiltered variability is even larger than predicted by the model. The stations at Hegyhatsal (Hungary) and the Tae-Ahn peninsula (Republic of Korea) are highly influenced by local processes. The former is a continental station primarily influenced by biogenic processes whereas the latter is located in the highly polluted area in East Asia. Nevertheless, the model is able to capture the measured variability rather well for both stations.

Summarising, the model performs well in predicting the measured mixing ratios at background and continental stations, both in the NH as well as in the SH. This suggests that the modelled  $H_2$  budget and the magnitudes of the different sources and sinks are reasonable. This provides an excellent starting-point for the evaluation of the isotopic

**Hydrogen isotope  
modelling**

G. Pieterse et al.

Title Page

Abstract

Introduction

Conclusions

References

Tables

Figures

◀

▶

◀

▶

Back

Close

Full Screen / Esc

Printer-friendly Version

Interactive Discussion



composition in the next section, where we will compare the modelled results with available data. The agreement between the model results and the measurements was also observed for 39 other sites in the NOAA and CSIRO network. The remaining comparisons are available on request from the corresponding author and in the supplementary material.

### 3.2 Comparison with H<sub>2</sub> isotope measurements

In Fig. 3, the latitudinal gradient of zonal mean values from the TM5 model is compared to measurements from Gerst and Quay (2000), Rice et al. (2010) and samples from the Eurohydros project (Batenburg et al., 2011). The results for the default scenario (thick solid line) show a systematic negative bias in the isotopic composition of about 10–15‰. This deviation is relatively small compared to the uncertainties in the fluxes and isotopic composition of the sources and sinks that contribute to the final isotopic composition (see Table 2). Furthermore, it should be noted that the measurements usually sample relatively clean background air, whereas the model averages over a latitude band and therefore usually also includes emissions from the isotopically depleted source regions over land. Thus, the available isotope measurements are not necessarily representative for the whole latitude band (i.e. the background isotope measurements are expected to be slightly more enriched) and therefore additional measurements at non-background locations (e.g. regions dominated by deposition or surface sources) are required to obtain a more consistent global latitudinal gradient. Overall, the comparison shows that the global isotope budget is already reasonably well described by the default model setup. The sensitivity of the results to a number of parameters is discussed in more detail in Sect. 3.6.

Figure 4 shows time series of the modelled (monthly averaged) and measured isotopic composition at the 6 Eurohydros flask stations (Batenburg et al., 2011) for the years 2006 and 2007. In general, the modelled isotope results are slightly depleted compared to the measurements, as discussed above. However the differences are not

## Hydrogen isotope modelling

G. Pieterse et al.

Title Page

Abstract

Introduction

Conclusions

References

Tables

Figures



Back

Close

Full Screen / Esc

Printer-friendly Version

Interactive Discussion



uniform between the stations. The largest underestimate is found at Neumayer. Here, the model also predicts a small but clear seasonal cycle with an amplitude of  $\sim 10\%$ , which is not discernible in the data. At Amsterdam Island, the discrepancy between model and data is somewhat reduced. Also at this station, the scatter in the data is too high to detect/verify a possible seasonal cycle. Cape Verde Island is the station where the model captures the measured values best. Unfortunately, the record for direct comparison is shortest, but the absolute values and the seasonal differences seem to be well represented by the model. The measurements at the continental station Schauinsland show the highest degree of variability due to influences from surface sources and deposition. The model averages out much of this variability and predicts a rather small and disturbed seasonal cycle. At Mace Head, the model captures the phase and amplitude of the seasonal cycle in 2007 very well, but again with a negative offset. Some measurements in summer 2006 appear anomalously high compared to the model and the 2007 record, but in general the agreement is very good. This deteriorates again when going to the high northern latitudes. Whereas the model predicts a rather similar seasonality as in Mace Head, the measurements show a shift in the phase for Alert. Direct comparison of the data for Alert and Mace Head in Fig. 4 shows that at the former station,  $\delta D[H_2]$  values increase again after the seasonal minimum 1–2 months earlier than at the latter station. Possibly, the phase shift in the modelled and measured seasonal signals at Alert is caused by the implementation of the deposition scheme for snow-covered conditions. In the current model deposition parametrisation, no deposition will occur in (partly) snow covered regions. It is therefore possible that in reality, deposition will start affecting the isotopic composition much earlier in the season than expected from the model results. Indeed, the mixing ratios for Alert in Fig. 1 already showed that the modelled seasonal minimum in the  $H_2$  mixing ratio is delayed compared to seasonal minimum in the observations by a similar number of months. Moreover, the modelled  $H_2$  seasonal minimum in the mixing ratio is significantly higher than the observed minimum mixing ratio, which leads to an underestimate in the modelled isotopic composition. Hence, more deposition measurements in continental regions

**Hydrogen isotope  
modelling**

G. Pieterse et al.

Title Page

Abstract

Introduction

Conclusions

References

Tables

Figures

◀

▶

◀

▶

Back

Close

Full Screen / Esc

Printer-friendly Version

Interactive Discussion



like Siberia (the area of influence for Alert) are required to improve our insight into the northern hemispheric H<sub>2</sub> cycle.

This qualitative comparison shows that there are potentially interesting isotope signals in the detailed records at individual measurement stations close to H<sub>2</sub> sources and sinks, but for the analysis in this paper we focus on the global values (e.g., Fig. 3). The difference between the model results and measurements appears limited for the tropics (Cape Verde), increases with latitude, and is more pronounced at the Southern Hemisphere. As in the tropics the photochemical production of H<sub>2</sub> is a strong source, the agreement suggests that the modelled tropospheric photochemical source signature is roughly realistic. However, one has to keep in mind that the global comparison also depends on the representativeness of the zonal average when compared to point measurements in the tropics. As the figures in the next section will show, there is a large variability caused by the sources and sinks in the tropics around the globe.

### 3.3 Analysis of spatial patterns

The left column in Fig. 5 shows the modelled latitude-altitude fields of H<sub>2</sub> mixing ratio for different seasons. Latitudinal, vertical and temporal variability is generally small in the southern extratropics. The H<sub>2</sub> mixing ratio in the tropics reaches a maximum during the northern hemispheric spring and summer, which penetrates deep into the free troposphere. In the northern extratropics, H<sub>2</sub> mixing ratios are lowest year-round and show a strong seasonal minimum in the fall season (SON). The vertical gradient is small in the Southern Hemisphere but quite substantial in the Northern Hemisphere, confirming earlier findings of Hauglustaine and Ehhalt (2002) and Price et al. (2007).

The corresponding isotope values are shown in the right column in Fig. 5. The dominant effect in this view is the strong isotope enrichment of H<sub>2</sub> in the stratosphere. This overshadows the smaller temporal and latitudinal changes in the troposphere. In general, the NH is isotopically depleted compared to the SH, as shown above. In the northern extratropics and tropics, there is generally only a weak vertical isotope gradient. Interestingly, when a vertical  $\delta D[H_2]$  gradient is observed in the NH, it is opposite

## Hydrogen isotope modelling

G. Pieterse et al.

Title Page

Abstract

Introduction

Conclusions

References

Tables

Figures

◀

▶

◀

▶

Back

Close

Full Screen / Esc

Printer-friendly Version

Interactive Discussion



**Hydrogen isotope  
modelling**

G. Pieterse et al.

Title Page

Abstract

Introduction

Conclusions

References

Tables

Figures

◀

▶

◀

▶

Back

Close

Full Screen / Esc

Printer-friendly Version

Interactive Discussion



to what is expected from deposition. The isotope effect in deposition leads to preferential removal of  $\text{H}_2$ , which would leave the atmosphere enriched in HD. However,  $\delta\text{D}[\text{H}_2]$  values near the surface are always lowest. Apparently, whereas deposition is clearly the driver for seasonality and vertical gradient of  $\text{H}_2$  mixing ratio in the NH, it has less effect on  $\delta\text{D}[\text{H}_2]$ . This is because the surface sources are strongly depleted in deuterium compared to the ambient reservoir, which overpowers the rather weak kinetic isotope effect in deposition. Surprisingly, on the seasonal scale, we see again an effect that is qualitatively in agreement again with the role of the sinks (mostly deposition, but some fraction of OH, see Batenburg et al., 2011). In SON, the  $\text{H}_2$  levels are lowest (due to depositional loss) and the  $\delta\text{D}[\text{H}_2]$  values are highest because HD remains preferentially in the atmosphere. So, deposition does affect the large-scale (temporal) evolution, but not the short-scale (vertical) distribution of  $\delta\text{D}[\text{H}_2]$ . It is noted however, that the inverse vertical gradient in the isotopic composition becomes less pronounced in the autumn season, when deposition reaches its maximum. This shows that deposition is indeed enriching the isotopic composition in the Northern Hemisphere.

In the SH, the isotope seasonality appears to be driven by an isotopic composition anomaly subsiding from a pressure altitude of 300 mbar at  $50^\circ$  south down to the surface pressure level at  $20^\circ$  south. It is strongest during the northern hemispheric winter (DJF) and spring season (MAM). The shape of this anomaly suggests a significant role of stratosphere-troposphere exchange (STE) on the isotopic composition in the SH. Apparently, in the NH such a signal is almost completely attenuated by the surface sources. The role of STE will be addressed in more detail by the sensitivity studies in Sect. 3.6.

The seasonal mean surface level  $\text{H}_2$  mixing ratios are shown in the left column of Fig. 6. The most prominent feature is the well-established strong inter-hemispheric gradient. Whereas there is relatively little seasonal variability in the SH, the NH is characterised by large seasonal variability. Figure 6 also shows that the NH is strongly influenced by the landmasses. In the extratropics (mostly in the NH, but also in the SH), in general lower  $\text{H}_2$  mixing ratios are observed over land than over the ocean.

This characteristic distribution is a consequence of the dominant role of the soil sink, which has the most prominent impact on the  $H_2$  mixing ratio during the autumn season (SON). In the Northern Hemisphere,  $H_2$  levels can also be much higher than the ocean background. These signals are related to fossil fuel burning in the highly populated regions or biomass burning in the tropics and near the borders between China and Siberia. These surface sources can produce strong  $H_2$  plumes that extend far over the ocean.

Looking at the isotopic composition (right column in Fig. 6) we can identify combustion processes by the clear  $\delta D[H_2]$  depletion. In particular the African and Asian tropical regions with high  $H_2$  mixing ratios and low isotopic composition are striking. Unfortunately, there are no data available to confirm these low  $\delta D[H_2]$  values, but the model captures the  $H_2$  measurements at the Tae-Ahn peninsula, Korea, well (see Fig. 2 in the previous section). Isotope measurements have been initiated to investigate whether  $\delta D[H_2]$  values  $<60\%$  actually occur. The precise  $\delta D[H_2]/H_2$  correlations should enable us to further constrain isotope source signatures in these regions.

On the global scale, the main  $\delta D[H_2]$  characteristic is again the inter-hemispheric gradient (right column in Fig. 6). The seasonal cycle of  $\delta D[H_2]$  in the SH is much smaller than in the NH, similar to the mixing ratios. Interestingly, the seasonality in the NH shows a delay in its response to the seasonal cycle of deposition, resulting in a seasonal maximum during the northern hemispheric autumn (SON) and winter (DJF) season, which is further explained in Sect. 3.4.

### 3.4 Global budget and isotope budget

The TM5 model keeps track of the total budget of the different chemical tracers. Although no explicit budget is calculated for the troposphere, the tropospheric budget can be estimated in a similar way as was presented by Ehhalt and Rohrer (2009). The overall budget for  $H_2$  is shown in Table 1, along with other recently published budget estimates. The magnitudes of the photochemical and deposition budget terms for the  $H_2$  mixing ratio are within the range of uncertainties of the previously reported budgets.

[Title Page](#)[Abstract](#)[Introduction](#)[Conclusions](#)[References](#)[Tables](#)[Figures](#)[◀](#)[▶](#)[◀](#)[▶](#)[Back](#)[Close](#)[Full Screen / Esc](#)[Printer-friendly Version](#)[Interactive Discussion](#)

Together with the good agreement between the model results and the measured H<sub>2</sub> mixing ratios (see Sect. 3.1), this confirms that the H<sub>2</sub> budget is well constrained.

The H<sub>2</sub> isotope budget for the atmosphere up to 100 mbar is shown in Table 2. Because the H<sub>2</sub> and HD mixing ratios in the stratosphere are parametrised (see Sect. 2.3), the corresponding budget terms are not easily interpreted. We calculate the flux weighted ratios and fractionation constants for the known budget terms and to calculate the overall isotopic composition using the following expression (Gerst and Quay, 2001):

$$\delta D[H_2] = \frac{1}{R_{VSMOW}} \frac{\sum_i w_i R_i}{\sum_j w_j \alpha_j} - 1. \quad (6)$$

In this expression,  $R_i$  are the source isotope ratios and  $\alpha_j$  are the sink fractionation constants (see Table 2).  $w_i$  and  $w_j$  are the corresponding relative weights. This budget calculation yields an average isotopic composition of +99‰. The modelled average tropospheric composition obtained from the mixing ratio fields is +128‰. This means that a contribution of +29‰ can be attributed to the stratosphere, a value similar to the value of +37‰ reported by Price et al. (2007).

The fractionation constants of the loss processes in Table 2 were obtained from the modelled H<sub>2</sub> and HD mixing ratios and fluxes by an approximation based on the Rayleigh distillation model for a single stage removal process  $j$  (Rayleigh, 1902):

$$\alpha_j \approx \frac{L_{HD,j} [H_2]_i}{L_{H_2,j} [HD]_i}, \quad (7)$$

where  $L_{HD,j}$  and  $L_{H_2,j}$  are the overall removal fluxes.  $[HD]_i$  and  $[H_2]_i$  are the burdens for HD and H<sub>2</sub> at the start of the simulation. The resulting effective fractionation for deposition (0.925) is stronger than the applied fractionation for the deposition (0.943) because the surface H<sub>2</sub> isotope composition is relatively light (i.e. H<sub>2</sub>/HD at the surface

Hydrogen isotope modelling

G. Pieterse et al.

Title Page

Abstract

Introduction

Conclusions

References

Tables

Figures

◀

▶

◀

▶

Back

Close

Full Screen / Esc

Printer-friendly Version

Interactive Discussion



Discussion Paper | Discussion Paper | Discussion Paper | Discussion Paper

where the removal fluxes are calculated is larger than  $H_2/HD$  averaged over the entire atmosphere, the value used for the budget calculation). The photochemical source signature of +116‰ is well within the ranges of  $+162_{-57}^{+57}$ ‰ and  $+130_{-70}^{+70}$ ‰ reported by Price et al. (2007) and Gerst and Quay (2001), respectively.

The average isotopic composition of +128‰ seems to be well within the range of values reported by Gerst and Quay (2001); Rahn et al. (2002b); Rhee et al. (2006); Price et al. (2007), however it is noted that the region of the atmosphere up to 100 mbar includes a large high latitude fraction of the stratospheric mass. This results in a significant positive bias towards the actual tropospheric value. Figure 3 in Sect. 3.2 already showed that the model underestimates the surface isotope measurements by approximately 10–15‰. Indeed, the budget for the lower troposphere (for pressure levels greater than 850 mbar) produces a value of +119‰. In Sect. 3.6 we will further investigate the sensitivity of the model results to changes in the parameters of the main processes in the  $H_2$  cycle and identify the opportunities for changing these parameters to close the gap between the measurements and the model results.

### 3.5 Global variability and isotope variability

For the purpose of investigating the global variability in more detail, the monthly atmospheric burden and fluxes of  $H_2$  and HD were integrated for three latitude bands,  $90^\circ S$ – $30^\circ S$ ,  $30^\circ S$ – $30^\circ N$ , and  $30^\circ N$ – $90^\circ N$ , respectively. The height of the three top box boundaries was set to 100 mbar. Figure 7 shows the resulting seasonal cycles in the  $H_2$  mixing ratio and isotopic composition in the three latitude bands.

This figure reproduces the established features of the global  $H_2$  cycle, for example the large seasonal cycle in the  $H_2$  mixing ratio in the Northern Hemisphere due to deposition (e.g., Novelli et al., 1999). To assess the variability in the mixing ratio and isotopic composition in the three different regions, all relevant processes should be considered, i.e. the emissions, photochemistry, deposition, horizontal advection, and vertical transport. We can analyse the  $H_2$  isotope budget in the model in more detail by calculating the contribution of each source and sink process individually to the change of the  $H_2$

## Hydrogen isotope modelling

G. Pieterse et al.

[Title Page](#)[Abstract](#)[Introduction](#)[Conclusions](#)[References](#)[Tables](#)[Figures](#)[◀](#)[▶](#)[◀](#)[▶](#)[Back](#)[Close](#)[Full Screen / Esc](#)[Printer-friendly Version](#)[Interactive Discussion](#)

mixing ratio and isotopic composition from one month to the next. The mathematical framework is derived in Appendix C, and the results are shown in Fig. 8.

Starting from a certain mixing ratio and isotopic composition for a given month in Fig. 7, the mixing ratio and isotopic composition of the next month will be changed by an amount equal to the sum of the contributions shown in Fig. 8. For example, surface emissions (red bars in Fig. 8) always constitute a net source and show up as a positive bar for the mixing ratio. However, these surface emissions are strongly isotopically depleted compared to the ambient reservoir, and therefore would lead to a decrease in the isotopic composition. In the model, these surface emissions have a strong seasonality in the extratropical boxes, but are rather constant in the tropics. Photochemical H<sub>2</sub> sources (green bars) can make a significant contribution to the total H<sub>2</sub> changes, especially in the tropics and the extratropical summer seasons, but the effect on the isotopic composition is negligible since the produced H<sub>2</sub> has an isotopic composition ( $\delta D[H_2] = 110\text{‰}$ ) very similar to the ambient reservoir.

The photochemical removal of H<sub>2</sub> at the higher NH latitudes shows up as a negative contribution to the mixing ratio change from one month to the next (light blue bars in Fig. 8). Although the photochemical removal is relatively small in magnitude, it is associated with strong isotope fractionation, clearly visible as a strong positive contribution to the change in isotopic composition. Deposition (dark blue bars) is a stronger source than photochemical removal, but the effect on the isotopic composition is overall smaller, since the isotope fractionation constant in soil deposition is much closer to unity.

Thus, Fig. 8 allows a detailed attribution of the impact of the different processes on the variability in the mixing ratio and isotopic composition of H<sub>2</sub>. The seasonal cycle of the isotopic composition in the higher northern latitudes is mainly determined by the photochemical loss of H<sub>2</sub>, deposition, and the surface emissions. As mentioned above, the photochemical source contributes has no “isotope leverage”, and only source processes with a significantly more enriched or depleted signature and sink processes will affect isotope variability. The seasonal cycle of the isotopic

**Hydrogen isotope  
modelling**

G. Pieterse et al.

Title Page

Abstract

Introduction

Conclusions

References

Tables

Figures

◀

▶

◀

▶

Back

Close

Full Screen / Esc

Printer-friendly Version

Interactive Discussion



composition at higher northern latitudes (see Fig. 7) is slightly shifted due to the different seasonality of the surface emissions (fossil fuel burning, biomass burning, and nitrogen fixation) compared to the seasonality of photochemistry and deposition. The small variability at tropical latitudes is mainly caused by slight variations in the surface emissions and the seasonal exchange with air masses from the Northern and Southern Hemispheres. The variability of the isotopic composition in the southernmost latitudes is mainly caused by seasonality in tropospheric photochemistry, counteracted by the surface emissions and the exchange of air with more depleted air from the tropical latitudes from June to September. The vertical flux is also an important term in the isotope budget of the southern latitudes during the winter season (JJA), in agreement with the results of the following sensitivity study. Having identified the most important processes, we will investigate the sensitivity of the model to actual changes in the parameters in the next section.

### 3.6 Sensitivity study

The previous sections showed that the modelled isotopic composition has a small negative bias compared to the available measurements. Different options for closing the discrepancy between the model results and the measurements are available and viable. In this section, we will investigate the sensitivity of the modelled isotopic composition to changes in the key parameters of the molecular hydrogen isotope cycle whilst keeping the  $H_2$  budget unaltered. In the methane and NMHC oxidation schemes, the final step towards the formation of  $H_2$  and HD, i.e. the destruction of formaldehyde ( $CH_2O$ ) is of large influence on the final isotopic composition (Feilberg et al., 2007a; Pieterse et al., 2009). Therefore the sensitivity of the isotopic composition upon changing the KIEs of the molecular and radical pathway of the two photolysis reactions of  $CH_2O$  was examined first. Case 1a (Table 3) employs the KIEs reported by Feilberg et al. (2007a). Evidently, the isotopic composition is very sensitive to changes in the KIEs for formaldehyde photolysis. As noted in Pieterse et al. (2009), the KIEs for the radical (R32b) and molecular (R33) photolysis removal channels for formaldehyde used

## Hydrogen isotope modelling

G. Pieterse et al.

Title Page

Abstract

Introduction

Conclusions

References

Tables

Figures

◀

▶

◀

▶

Back

Close

Full Screen / Esc

Printer-friendly Version

Interactive Discussion



for this case lead to a significant underestimation of the isotopic composition.

Case 1b tests the sensitivity of the isotopic composition to changes in the pressure dependency of the KIE of reaction R33b and leads to a large increase in isotopic composition of 18‰. Thus, the tropospheric composition shows a significant sensitivity to changes in the pressure dependency of the molecular photolysis removal channel for formaldehyde, especially in the tropics, as shown in the zonal annual mean difference plot in Fig. 9.

The sensitivity of the tropospheric composition to changes in the stratospheric parametrisation was tested by increasing the isotopic composition in the stratosphere by 20‰ compared to the default scenario (case 2a). The effect on the average tropospheric composition is profound (an increase of 12‰). Evidently, H<sub>2</sub> produced in the stratosphere is highly enriched (Rahn et al., 2003; Röckmann et al., 2003) and is an important potential enriching process in the atmospheric budget, as was already concluded from the results in Table 2 and Fig. 8 in Sect. 3.4. The sensitivity of the model to changes in the stratospheric parametrisation was further investigated by changing Eq. (1) in Sect. 2.3 (case 2b and 2c). The cases were carefully chosen to distinguish between the STE at higher latitudes (2b) and (2c) the STE near the tropical tropopause/transition layer (TTL). Both cases show that the isotopic composition is also sensitive to changes in the pressure levels above which the parametrisation described in Sect. 2.3 is used. Changes near the TTL were not expected to affect tropospheric composition because H<sub>2</sub> is photochemically produced in this region and then transported upwards into the stratosphere. Indeed, the results of case 2b and 2c show similar effects on the tropospheric isotopic composition, both in magnitude as well as distribution (see Fig. 9). Thus, heavy H<sub>2</sub> is injected from the mid-latitude stratosphere into the troposphere (e.g., Reid and Vaughan, 1991; Appenzeller et al., 1996; Lelieveld et al., 1997; Hintsä et al., 1998; Dethof et al., 2000). This effect is also clearly visible in the zonal mean isotopic composition during the NH winter and spring season shown in Fig. 5, and is more pronounced in the Southern Hemisphere because in the Northern Hemisphere it is damped by the seasonality in the surface emissions (see Fig. 8)

## Hydrogen isotope modelling

G. Pieterse et al.

Title Page

Abstract

Introduction

Conclusions

References

Tables

Figures

◀

▶

◀

▶

Back

Close

Full Screen / Esc

Printer-friendly Version

Interactive Discussion



resulting in less enrichment.

Figure 3 shows that increasing the isotopic composition at and above the tropopause by 20‰ closes the gap between the default scenario isotopic composition and the observations. It is noted however that previous studies have shown that the Brewer-Dobson circulation is overestimated by the meteorological data from ECMWF and consequently the downward transport from the stratosphere to the troposphere is a factor 2–3 too high, at least for ozone (van Noije et al., 2004, 2006). This could mean that the actual downward transport of heavy hydrogen (i.e. the contribution to the isotope budget) might be significantly lower than predicted by the TM5 model. However, the effect of the stratosphere on the tropospheric isotopic composition of H<sub>2</sub> was also observed by Price et al. (2007) who used another global chemical transport model (CTM) driven by a different meteorology; The stratospheric contribution to the tropospheric isotopic composition computed in the current study (+29‰) is similar to their calculated contribution of +37‰, calculated using the GEOS-chem CTM. Thus, the STE is considered a potentially important process for the tropospheric isotope budget of H<sub>2</sub> in both studies available to date. Measuring the isotopic composition at the tropopause and in the lower stratosphere is therefore important to obtain a crucial boundary condition for the tropospheric model simulations.

Case 3 was chosen to investigate the sensitivity of the model results to the initial isotopic compositions of the NMHCs participating in the H<sub>2</sub> cycle. The full NMHC hydrogen isotope chemistry mechanism consists of a large set of chemical reactions and is poorly constrained by available measurements. We believe that with so many unverified parameters, a comprehensive sensitivity study of the mechanism would not be of value at this time. Therefore, we chose to test the sensitivity of the isotopic composition to changes in the initial isotopic composition from –86‰ to –200‰. The result (a decrease of 10‰) in Table 3 shows that the model is indeed sensitive to changing the isotopic composition of the NMHCs, although it is noted that the applied perturbation was large (a decrease of 114‰) and the effect is relatively small (see Fig. 9).

## Hydrogen isotope modelling

G. Pieterse et al.

Title Page

Abstract

Introduction

Conclusions

References

Tables

Figures

◀

▶

◀

▶

Back

Close

Full Screen / Esc

Printer-friendly Version

Interactive Discussion



In the fourth set of cases, the sensitivity of the model output on the isotopic composition of the surface sources is investigated. For case 4a, we implemented an isotopic source signature of  $-700\%$  for terrestrial and oceanic nitrogen fixation processes. This value was adopted from Rahn et al. (2003) where it was derived for the nitrogen fixation emissions from the oceans assuming thermodynamic equilibrium between  $H_2$  and  $H_2O$ . The observed change given in Table 3 is small, as was to be expected from the isotope budget shown in Table 2 in Sect. 3.4. Hence, the model results are not very sensitive to changes. For case 4b, we lowered the isotopic source signature of the fossil fuel sources to  $-250\%$ . The new value is the average of the values for incomplete and full catalytic conversion of exhaust fumes, recently reported by Vollmer et al. (2010). The difference will be only noticeable in highly populated areas because of the more intensive fossil fuel usage. On the global scale, however, the isotopic composition is barely affected by the change in source signature. With case 4c, we investigated the sensitivity of the model results to a change in the isotopic signature of the biomass burning emissions to the value suggested by Gerst and Quay (2001). Again, the global signals of the isotopic composition are not significantly altered by the different source signature. Thus, for all sub-scenarios of case 4, the previously reported ranges of uncertainty in the source signatures do not lead to a significant uncertainty in the global isotopic composition. This implies that the available surface source signatures are sufficiently constrained to close the global  $H_2$  isotope budget, although more accurate values might be required to close the regional budgets.

With case 5, we investigated the sensitivity of the model to changes in the fractionation constant for deposition from 0.943 to 0.900 (see Fig. 10). Because deposition is the largest sink for  $H_2$ , a large effect was to be expected for a perturbation on the fractionation constant well outside the reported range of  $\pm 1\sigma$  uncertainty of  $0.943 \pm 0.024$  (Gerst and Quay, 2001). Hence, the regional isotope budgets, especially above the Eurasian continent, appear very sensitive to small changes in the fractionation associated with deposition.

**Hydrogen isotope  
modelling**

G. Pieterse et al.

Title Page

Abstract

Introduction

Conclusions

References

Tables

Figures

◀

▶

◀

▶

Back

Close

Full Screen / Esc

Printer-friendly Version

Interactive Discussion



In conclusion, three cases provide good opportunities to reduce the bias between the modelled and measured gradient. Case 1b shows that implementing a different pressure sensitivity of R33 could solve the bias between the modelled and measured global isotopic composition. Also, an increase of 20‰ in the isotopic composition at the tropopause (case 2a) could suffice. Finally, case 5 reduces the difference by employing a lower fractionation constant for deposition (0.900 in stead of 0.943). It is clear that the parameters of case 1b and 5 were perturbed outside the reported ranges of uncertainty. Nevertheless, a combination of changes within range of uncertainty of the involved parameters will resolve the bias between the modelled and measured isotopic composition (see Fig. 3 in Sect. 3.2). Another way to try to close the isotope budget is to implement photochemical NMHC sources of H<sub>2</sub> that are not yet considered in the TM5 model, e.g. the methanol emissions or the chemistry of the monoterpenes. These options were not considered here because exploratory budget calculations showed that this would not close the gap between the measurements and the model results.

## 4 Conclusions

We have implemented H<sub>2</sub> sources and sinks, including isotopic composition, and a simplified but explicit isotope photochemistry scheme into the TM5 global chemistry transport model. The modelled H<sub>2</sub> mixing ratios were compared with available measurements. On the seasonal and inter-annual time scale, the modelled mixing ratios were found to be in good agreement with all observations. The global budget also showed that the model adequately reproduces the established values for the tropospheric burden and atmospheric lifetime of H<sub>2</sub> (155 Tg H<sub>2</sub> and 2.0 years, respectively). In all, the model provides a very adequate description of the global H<sub>2</sub> cycle.

The modelled isotopic composition was compared with available observations and the mean zonal gradient of the modelled surface isotopic composition shows a consistent negative bias of approximately 10–15‰. The uncertainties in the available isotope measurements are significant and provide room for model parameter adjustments

## Hydrogen isotope modelling

G. Pieterse et al.

Title Page

Abstract

Introduction

Conclusions

References

Tables

Figures

◀

▶

◀

▶

Back

Close

Full Screen / Esc

Printer-friendly Version

Interactive Discussion



**Hydrogen isotope  
modelling**

G. Pieterse et al.

Title Page

Abstract

Introduction

Conclusions

References

Tables

Figures

◀

▶

◀

▶

Back

Close

Full Screen / Esc

Printer-friendly Version

Interactive Discussion



within their range of uncertainty without changing the source and sink magnitudes. However, the observed latitudinal gradient in the isotopic composition constrains the possibilities of closing the  $H_2$  isotope budget on a global scale to a limited number of parameters. In a comprehensive sensitivity study (see Sect. 3.6) several parameters were identified as possible candidates to explain the bias between the model and observations: the missing NMHC emissions of e.g. the monoterpenes and methanol, the KIE of the molecular channel of the photolysis reaction of formaldehyde, the fractionation constant for deposition, and finally the isotopic composition around the tropopause used as an upper boundary condition for the calculations.

Interestingly, the TM5 model results are very sensitive to the tropopause boundary height above which the stratospheric parametrisation described by McCarthy et al. (2004) is used. Although the STE flux of  $H_2$  is small in magnitude compared to other fluxes that determine the tropospheric  $H_2$  isotope budget, its source signature is significantly enriched. Price et al. (2007) already reported that the stratosphere appears to enrich the troposphere by an amount of 37%. This value is close to the 29% found in the present study, even though different meteorological data are used to drive the transport in the two models. These findings suggest that the stratosphere-troposphere exchange (STE) might be an important process for the tropospheric  $H_2$  isotope budget, although it is noted that both models use the parametrisation by McCarthy et al. (2004) and might be similarly affected by shortcomings in this parametrisation, if any. Tropospheric surface measurements of the isotopic composition will not discern between  $H_2$  photochemically produced in the troposphere or the stratosphere, and therefore the significance of the stratospheric impact might pass unnoticed.

As the isotopic composition is calculated including a full isotope chemistry scheme, it is also possible to study the isotopic budgets of chemical precursors. We consider the isotope budget of formaldehyde ( $CH_2O$ ) as an important tool to evaluate the impact of the different photochemical processes on the final isotopic composition of  $H_2$ , and to improve the model using available measurements. This will be the subject of future research. The available isotope data do not provide sufficient information to uniquely

constrain the global isotope budget. The background isotope measurements do not contain all information required to constrain the global isotope budget and their use might introduce biases. Additional studies further focussing on the isotope effects in the photochemistry and deposition in non background conditions as well as studies focussing on the isotopic composition near the tropopause are therefore recommended.

## Appendix A

### Derivation of the methane reaction mechanism

The new methane related reactions implemented in the TM5 model are shown in Table A1. To enable unambiguous reference to the original CBM-4 scheme (Houweling et al., 1998), we chose to use the original reaction numbering. Methane background mixing ratio fields obtained using the four-dimensional variational (4-D-Var) data assimilation system implemented in TM5 (Meirink et al., 2008a,b) are used to prescribe the CH<sub>4</sub> mixing ratio fields. Budget calculations with the TM5 model configuration presented in this work yield an overall atmospheric life time of 8.7 years for methane, a value very similar to the 8.4 years reported by Houghton et al. (2001). This correspondence implies realistic values for the mixing ratios of the hydroxyl radical (OH), a species that is also responsible for the removal of H<sub>2</sub>. The mixing ratio of the singly deuterated methane isotopologue (CH<sub>3</sub>D) is fixed by asserting a uniform isotopic composition of -86‰ for the entire atmosphere, which is justified because the observed atmospheric variability is small (Quay et al., 1999), neglecting spatial and temporal variability.

## Hydrogen isotope modelling

G. Pieterse et al.

Title Page

Abstract

Introduction

Conclusions

References

Tables

Figures

◀

▶

◀

▶

Back

Close

Full Screen / Esc

Printer-friendly Version

Interactive Discussion



## A1

### Reaction of methane (CH<sub>4</sub>)

The KIE of the reaction of the methane isotopologues (R26a and R26b) directly follows from the recommendations in Sander et al. (2006). The branching ratio was calculated following the method discussed previously by Pieterse et al. (2009).

$$\alpha_{\text{CH}_3\text{D}+\text{OH}}^{\text{D}} = \frac{3}{4} \text{KIE}_{\text{CH}_4+\text{OH}} \quad (\text{A1})$$

In this reaction,  $\text{KIE}_{\text{CH}_4+\text{OH}}$  is calculated as the ratio between the rate coefficient of the deuterated and the non deuterated methane isotopologue. Because this ratio is temperature dependent, the branching ratio is also temperature dependent and therefore it is calculated online. TM5 does not consider the intermediate methyl radical CH<sub>3</sub> and immediately forms the methylperoxy radical (CH<sub>3</sub>OO) via O<sub>2</sub> addition, as described for example in Ravishankara (1988). It is assumed that isotope effects in this fast intermediate reaction are negligible.

## A2

### Reactions of the methylperoxy radical (CH<sub>3</sub>O<sub>2</sub>)

The reaction of CH<sub>3</sub>OO with nitric oxide (NO) forms the methoxy radical (CH<sub>3</sub>O). A possible hydrogen isotope effect in this reaction will likely be very small since hydrogen atoms are not directly involved, therefore it is neglected. The reaction of the methoxy radical with O<sub>2</sub> forms formaldehyde (CH<sub>2</sub>O). This hydrogen abstraction reaction has a strong KIE of 1.323 (e.g., Nilsson et al., 2007) and a significant isotopic branching (IB) ratio, i.e. 0.882, which strongly affect the isotopic composition of formaldehyde (CH<sub>2</sub>O). In the TM5 model, the methoxy radical is not implemented and the sequence of the two elementary reactions is condensed into reaction R27. In the absence of temperature

Title Page

Abstract

Introduction

Conclusions

References

Tables

Figures

◀

▶

◀

▶

Back

Close

Full Screen / Esc

Printer-friendly Version

Interactive Discussion



dependent data at the time of this study, the KIE and IB ratio are assumed constant for the entire atmosphere.

The methylperoxy radical also combines with the hydroperoxy radical ( $\text{HO}_2$ ), via reaction R28. Because the hydrogen atom of  $\text{HO}_2$  is added to the peroxy group, and the deuteron in the methyl group of  $\text{CH}_3\text{OO}$  is not directly involved directly in the formation of methyl hydroperoxide ( $\text{CH}_3\text{O}_2\text{H}$ ), the KIE and IB ratio are set equal to unity.

The last removal mechanism of  $\text{CH}_3\text{OO}$  that is implemented in TM5 is its self reaction (R29). Although the isotope effects in the primary reaction are very likely small, there are several subsequent reactions via methanol ( $\text{CH}_3\text{OH}$ ) for which isotope effects must be considered (DeMore et al., 1994; Sander et al., 2006; Pieterse et al., 2009). The fraction of deuterons that ends up in the final reservoir species formaldehyde is not straightforward to calculate. Pieterse et al. (2009) implemented the intermediate steps following the initial self reaction, shown in Table A2.

Using the IB ratios and KIEs in this table (also derived by Pieterse et al., 2009), the overall KIE and IB ratio for reaction R29b in Table A1 are calculated as follows:

$$\begin{aligned} \text{IB} &= \text{IB}[\text{B1b}_1] \cdot \text{IB}[\text{B4b}_1] + \text{IB}[\text{B1b}_2] \cdot (\text{IB}[\text{B2b}_1] \cdot \text{IB}[\text{B4b}_1] + \text{IB}[\text{B2b}_2] \cdot \text{IB}[\text{B3c}]) \\ &= 0.810, \end{aligned} \tag{A2}$$

and:

$$\begin{aligned} \text{KIE} &= \text{KIE}[\text{B1b}] \cdot \text{IB}[\text{B1b}_1] \cdot \text{KIE}[\text{B4b}] + \\ &\quad \text{KIE}[\text{B1b}] \cdot \text{IB}[\text{B1b}_2] \cdot \text{KIE}[\text{B2b}] \cdot (\text{IB}[\text{B2b}_1] \cdot \text{KIE}[\text{B4b}] + \text{IB}[\text{B2b}_2] \cdot \text{KIE}[\text{B3c}]) + \\ &\quad \text{KIE}[\text{B1b}] \cdot \text{IB}[\text{B1b}_3] \\ &= 1.221. \end{aligned} \tag{A3}$$

## Hydrogen isotope modelling

G. Pieterse et al.

Title Page

Abstract

Introduction

Conclusions

References

Tables

Figures

◀

▶

◀

▶

Back

Close

Full Screen / Esc

Printer-friendly Version

Interactive Discussion



### A3

#### Reactions of methyl hydroperoxide (CH<sub>3</sub>O<sub>2</sub>H)

Methyl hydroperoxide is oxidised with OH (R30) via two channels, one forming a CH<sub>3</sub>OO radical and the other forming a CH<sub>2</sub>O<sub>2</sub>H radical that immediately dissociates to formaldehyde. The photochemical destruction of methyl hydroperoxide produces CH<sub>3</sub>O that reacts to formaldehyde with oxygen. The values for the IB ratios and the KIE for these two reactions were taken from Pieterse et al. (2009).

### A4

#### Reactions of formaldehyde (CH<sub>2</sub>O)

The removal reactions of formaldehyde are the most crucial for correct hydrogen isotope modelling (Feilberg et al., 2007a; Rhee et al., 2008; Pieterse et al., 2009; Nilsson et al., 2009; Röckmann et al., 2010). In the study by Feilberg et al. (2007a) an overall KIE for the photolysis of 1.58 was found, and values of 1.82 and 1.10 were reported for the molecular channel and radical channel, respectively. However, the exact isotope effects in the two individual photolysis reactions (R32 and R33) are still subject of discussion (Pieterse et al., 2009). The reported KIEs lead to a significant mismatch between the actual relative magnitudes of the two photochemical pathways when matched to the overall KIE. New experimental data suggest that the KIE of the molecular channel is pressure dependent:

$$\text{KIE} = \frac{500.00 + 2.50 \times 10^{-2}p}{500.00 + 1.34 \times 10^{-2}p}, \quad (\text{A4})$$

with the pressure  $p$  in Pa (Nilsson et al., 2009) where these parameters have been slightly adjusted to a value of 1.63 at atmospheric pressure (Röckmann et al., 2010). These data also suggest that the KIE of the radical channel should be much closer

Title Page

Abstract

Introduction

Conclusions

References

Tables

Figures

◀

▶

◀

▶

Back

Close

Full Screen / Esc

Printer-friendly Version

Interactive Discussion



to the KIE of the molecular channel than postulated by Feilberg et al. (2007a) and Rhee et al. (2008). In absence of established experimental values we adapted a KIE of 1.580 for the radical channel. The KIE for the removal reaction of formaldehyde by OH oxidation (R34) was adopted from Feilberg et al. (2004) and set to 1.280. No kinetic isotope effects are implemented for the reaction of formaldehyde with NO<sub>3</sub> (R35) because of its minor importance in the global H<sub>2</sub> budget.

## Appendix B

### Derivation of the NMHC reaction mechanism

The reaction mechanism for the NMHC's used for this work is shown in Table B1. In this table, ALD2 represents acetaldehyde and higher aldehydes, C<sub>2</sub>O<sub>3</sub> is the peroxyacetyl radical, PAN represents the peroxyacetyl nitrate and higher PANs, PAR are the paraffinic carbon atoms, OLE are the olefinic carbon bonds, ETH are the alkenes, MGLY is methylglyoxal, ISOP is isoprene, ROOH represents the lumped organic peroxides (> C<sub>1</sub>), ORGNIT represents the lumped alkyl nitrates, XO<sub>2</sub> is the NO to NO<sub>2</sub> operator, XO<sub>2</sub>N is the NO to alkyl nitrate operator, and finally RXPAN is PAR budget corrector. Because experimental data on the full NMHC oxidation chain are not available, and because the isotope effects in the oxidation of singly deuterated NMHCs such as isoprene are expected to be small (e.g., Atkinson et al., 2006; McCaulley et al., 1989), we chose not to incorporate kinetic isotope effects in the standard model parameters at this time (i.e. KIE = 1.000 for all reactions) and subsequently, branching is treated purely statistical.

The branching ratios of the removal reactions of the olefins (OLE), alkenes (ETH), and isoprene (ISOP) by OH, O<sub>3</sub>, and NO<sub>3</sub> (R49 to R53, R56 to R58) were adopted from Pieterse et al. (2009). Because of the comparable initial amount of hydrogen atoms, the branching ratios of the oxidation and photolysis reactions of acetaldehyde and higher aldehydes (R38 and R39) are assumed to be equal to the branching ratios of

## Hydrogen isotope modelling

G. Pieterse et al.

[Title Page](#)[Abstract](#)[Introduction](#)[Conclusions](#)[References](#)[Tables](#)[Figures](#)[◀](#)[▶](#)[◀](#)[▶](#)[Back](#)[Close](#)[Full Screen / Esc](#)[Printer-friendly Version](#)[Interactive Discussion](#)

ETH and OLE (0.500). The reactions of the important intermediate peroxyacetyl radical ( $C_2O_3$ ) with  $NO$ ,  $C_2O_3$  and  $HO_2$ , leading to formaldehyde and  $XO_2$  in the original CBM-4 scheme (R40, R44, and R45, respectively) were altered to produce  $CH_3OO$  instead. This way, the isotope and branching effects in the remaining reactions towards  $H_2$  are taken into account appropriately. The involved reactions are shown schematically in Fig. B1.

## Appendix C

### Derivation of expressions to analyse the variability in the $H_2$ budget

The variability in the  $H_2$  budget can be analysed by taking the time derivative of the definition expression for the  $H_2$  mixing ratio:

$$\frac{d[H_2]}{dt} = \frac{M_{air}}{M_{H_2}} \left( \frac{1}{m_{air}} \frac{dm_{H_2}}{dt} - \frac{m_{H_2}}{m_{air}^2} \frac{dm_{air}}{dt} \right), \quad (C1)$$

where  $M_{air}$  and  $M_{H_2}$  are the molar mass of air and  $H_2$ . Furthermore,  $m_{air}$  and  $m_{H_2}$  are the overall air and  $H_2$  masses in the budget domains. Note that the seasonal change in the overall air mass should be considered when studying the variability in the mixing ratio. We have combined this effect into the default horizontal transport budget term in the  $H_2$  budget because it is related to the seasonal cycles in surface pressure (as a result of the seasonal cycle in temperature) above the oceans and continents in the NH and SH that also cause horizontal transport. In general, the change in the  $H_2$  budget mass can be calculated using  $n$  budget fluxes for the sources and sinks, resulting in the following expression:

$$\frac{d[H_2]}{dt} = \frac{M_{air}}{M_{H_2}} \left( \frac{1}{m_{air}} \sum_{i=0}^{n-1} \frac{dm_{H_2,i}}{dt} - \frac{m_{H_2}}{m_{air}^2} \frac{dm_{air}}{dt} \right). \quad (C2)$$

Title Page

Abstract

Introduction

Conclusions

References

Tables

Figures

◀

▶

◀

▶

Back

Close

Full Screen / Esc

Printer-friendly Version

Interactive Discussion



Similarly, we can investigate the variability in the isotope budget of H<sub>2</sub> by using the definition for the isotope ratio:

$$R \equiv \frac{[\text{HD}]}{[\text{H}_2]}, \quad (\text{C3})$$

to obtain its time derivative in the following form:

$$\frac{dR}{dt} = \frac{1}{[\text{H}_2]} \frac{d\text{HD}}{dt} - \frac{[\text{HD}]}{[\text{H}_2]^2} \frac{d\text{H}_2}{dt}. \quad (\text{C4})$$

In general, the time derivatives of the H<sub>2</sub> and HD mixing ratios are equal to the sum of  $n$  fluxes that can be positive or negative for each of the two isotopologues, also dependent on time. Hence, Eq. C4 reduces to:

$$\frac{dR}{dt} = \sum_{i=0}^{n-1} \left( \frac{1}{[\text{H}_2]} P_{\text{HD},i} - \frac{[\text{HD}]}{[\text{H}_2]^2} P_{\text{H}_2,i} + \frac{[\text{HD}]}{[\text{H}_2]} (k_{\text{H}_2,i} - k_{\text{HD},i}) \right). \quad (\text{C5})$$

In this expression,  $P_{\text{H}_2,i}$  and  $P_{\text{HD},i}$  are the production fluxes of H<sub>2</sub> and HD, respectively. The variables  $k_{\text{H}_2,i}$  and  $k_{\text{HD},i}$  are the removal rate coefficients. The impact of source, sink, and bi-directional processes on the variability in the isotope ratio can now be calculated in terms of equally scaled contributions. Moreover, the extension to the delta-notation is straightforward:

$$\frac{d}{dt} \delta\text{D}[\text{H}_2] = \frac{d}{dt} \left( \frac{R}{R_{\text{VSMOW}}} - 1 \right) = \frac{1}{R_{\text{VSMOW}}} \frac{dR}{dt}. \quad (\text{C6})$$

**Supplementary material related to this article is available online at:**  
<http://www.atmos-chem-phys-discuss.net/11/5811/2011/acpd-11-5811-2011-supplement.pdf>.

Title Page

Abstract

Introduction

Conclusions

References

Tables

Figures

◀

▶

◀

▶

Back

Close

Full Screen / Esc

Printer-friendly Version

Interactive Discussion



*Acknowledgements.* This study was funded by the Dutch NWO-ACTS project 053.61.026 and by the Eurohydros project, via the Sixth Framework Programme of the European Union (SUSTDEV-2005-3.I.2.1 Atmospheric composition change: Methane, Nitrous Oxide and Hydrogen). Andrew Rice from Portland State University (USA) and Paul Quay from the University of Washington (USA) are acknowledged for access to their H<sub>2</sub> isotope data. Paul Novelli from NOAA/CMDL (USA) provided the H<sub>2</sub> measurement data used for the validation of the modelled H<sub>2</sub> mixing ratios. We would like to thank Laurens Ganzeveld from Wageningen University (NL) for help with the implementation of the dry deposition parametrisation. Finally, the National Computing Facilities foundation (NCF) is acknowledged for providing the computational facilities to run the TM5 model.

## References

- Appenzeller, C., Davies, H. C., and Norton, W. A.: Fragmentation of stratospheric intrusions, *J. Geophys. Res.*, 101(D1), 1435–1456, doi:10.1029/95JD02674, 1996. 5830
- Atkinson, R.: Gas-phase tropospheric chemistry of organic compounds, *J. Phys. Chem. Ref. Data Monogr.*, 2, 1–216, 1994. 5855
- Atkinson, R., Baulch, D. L., Cox, R. A., Hampson, R. F., Kerr, J. A., and Troe, J.: Evaluated kinetic and photochemical data for atmospheric chemistry: supplement IV, *Atmos. Environ.*, 26, 1187–1230, 1992. 5853
- Atkinson, R., Baulch, D. L., Cox, R. A., Crowley, J. N., Hampson, R. F., Hynes, R. G., Jenkin, M. E., Rossi, M. J., Troe, J., and IUPAC Subcommittee: Evaluated kinetic and photochemical data for atmospheric chemistry: Volume II – gas phase reactions of organic species, *Atmos. Chem. Phys.*, 6, 3625–4055, doi:10.5194/acp-6-3625-2006, 2006. 5839
- Batenburg, A. et al.: in preparation, 2011. 5815, 5821, 5824, 5858
- van den Broek, M. M. P., van Aalst, M. K., Bregman, A., Krol, M., Lelieveld, J., Toon, G. C., Garcelon, S., Hansford, G. M., Jones, R. L., and Gardiner, T. D.: The impact of model grid zooming on tracer transport in the 1999/2000 Arctic polar vortex, *Atmos. Chem. Phys.*, 3, 1833–1847, doi:10.5194/acp-3-1833-2003, 2003. 5816
- Brühl, C. and Crutzen, P. J.: MPIC two dimensional model, *NASA Ref. Publ.*, 1292, 103–104, 1992. 5853

## Hydrogen isotope modelling

G. Pieterse et al.

Title Page

Abstract

Introduction

Conclusions

References

Tables

Figures

◀

▶

◀

▶

Back

Close

Full Screen / Esc

Printer-friendly Version

Interactive Discussion



- Conrad, R. and Seiler, W.: Contribution of hydrogen production by biological nitrogen fixation to the global hydrogen budget, *J. Geophys. Res.*, 85(C10), 5493–5498, 1980. 5818
- Conrad, R. and Seiler, W.: Influence of temperature, moisture, and organic carbon on the flux of H<sup>2</sup> and CO between soil and atmosphere: field studies in subtropical regions, *J. Geophys. Res.*, 90, 5699–5709, 1985. 5818
- DeMore, W. B., Sander, S. P., Golde, D. M., Hampson, R. F., Kurylo, M. J., Howard, C. J., Ravishankara, A. R., Kolb, C. E., and Molina, M. J.: Chemical kinetics and photochemical data for use in stratospheric modelling, evaluation number 11, Technical report, JPL Publication 94-26, Jet Propulsion Laboratory, Pasadena, 1994. 5837, 5853, 5855
- Dethof, A., O'Neill, A., and Slings, J.: Quantification of the isentropic mass transport across the dynamical tropopause, *J. Geophys. Res.*, 105(D10), 12279–12293, doi:10.1029/2000JD900127, 2000. 5830
- Ehhalt, D. H.: Gas phase chemistry of the troposphere, in global aspects of atmospheric chemistry, in: *Topics Phys. Chem.*, Vol. 6, edited by: Zellner, R., Springer-Verlag, New York, 21–109, 1999. 5813
- Ehhalt, D. H. and Rohrer, F.: The tropospheric cycle of H<sub>2</sub>: a critical review, *Tellus B*, 61(3), 500, doi:10.1111/j.1600-0889.2009.00416.x, 2009. 5813, 5818, 5825
- Feck, T., Groß, J.-U., and Riese, M.: Sensitivity of Arctic ozone loss to stratospheric H<sub>2</sub>O, *Geophys. Res. Lett.*, 35, L01803, doi:10.1029/2007GL031334, 2008. 5813
- Feilberg, K. L., Johnson, M. S., and Nielsen, C. J.: Relative reaction rates of HCHO, HCDO, DCDO, H<sup>13</sup>CHO, and HCH<sup>18</sup>O with OH, Cl, Br, and NO<sub>3</sub> radicals, *J. Phys. Chem. A*, 108, 7393–7398, 2004. 5813, 5814, 5839
- Feilberg, K. L., D'Anna, B., Johnson, M. S., and Nielsen, C. J.: Relative tropospheric photolysis rates of HCHO, H<sup>13</sup>CHO, HCH<sup>18</sup>O, and DCDO measured at the european photoreactor facility (EUPHORE), *J. Phys. Chem. A*, 109, 8314–8319, 2005. 5813, 5814
- Feilberg, K. L., Johnson, M. S., Bacak, A., Röckmann, T., and Nielsen, C. J.: Relative tropospheric photolysis rates of HCHO and HCDO measured at the European photoreactor facility, *J. Phys. Chem. A*, 111, 9034–9036, 2007a. 5813, 5814, 5829, 5838, 5839, 5858
- Feilberg, K. L., D'Anna, B., Johnson, M. S., and Nielsen, C. J.: Relative tropospheric photolysis rates of HCHO, H<sup>13</sup>CHO, HCH<sup>18</sup>O, and DCDO measured at the european photoreactor facility (EUPHORE), *J. Phys. Chem. A*, 111(5), 992, 2007b. 5813, 5814
- Ganzeveld, L. and Lelieveld, J.: Dry deposition parameterization in a chemistry general circulation model and its influence on the distribution of reactive trace gases, *J. Geophys. Res.*,

**Hydrogen isotope  
modelling**

G. Pieterse et al.

Title Page

Abstract

Introduction

Conclusions

References

Tables

Figures

◀

▶

◀

▶

Back

Close

Full Screen / Esc

Printer-friendly Version

Interactive Discussion



**Hydrogen isotope  
modelling**

G. Pieterse et al.

Title Page

Abstract

Introduction

Conclusions

References

Tables

Figures

◀

▶

◀

▶

Back

Close

Full Screen / Esc

Printer-friendly Version

Interactive Discussion



- 100(D10), 20999–21012, 1995. 5819
- Ganzeveld, L., Lelieveld, J., and Roelofs, G.-J.: A dry deposition parameterization for sulfur oxides in a chemistry and general circulation model, *J. Geophys. Res.*, 105(D5), 5679–5694, doi:10.1029/97JD03077, 1998. 5818, 5819
- 5 Garland, J. A.: The dry deposition of sulphur dioxide to land and water surfaces, *P. R. Soc. London*, A354, 245–268, 1977. 5818
- Gerst, S. and Quay, P.: The deuterium content of atmospheric molecular hydrogen: method and initial measurements, *J. Geophys. Res.*, 105, 26433–26445, 2000. 5821, 5858
- Gerst, S. and Quay, P.: Deuterium component of the global molecular hydrogen cycle, *J. Geophys. Res.*, 106, 5021–5031, 2001. 5813, 5814, 5819, 5826, 5827, 5832
- 10 Gery, M. W., Whitten, G. Z., Killus, J. P., and Dodge, M. C.: Development and testing of the CBM-4 for urban and regional modelling, Technical Report Rep. EPA-600/3-88-012, US Environ. Prot. Agency, Research Triangle Park, NC, 1988. 5855
- Gery, M. W., Whitten, G. Z., Killus, J. P., and Dodge, M. C.: A photochemical kinetics mechanism for urban and regional scale computer modeling, *J. Geophys. Res.*, 94(12), 12925–12956, 1989. 5855
- 15 Hauglustaine, D. A. and Ehhalt, D. H.: A three-dimensional model of molecular hydrogen in the troposphere, *J. Geophys. Res.*, 4330, 107, doi:10.1029/2001JD001156, 2002. 5813, 5818, 5823
- 20 Hertel, O., Berkowicz, R., Christensen, J., and Hov, O.: Test of two numerical schemes for use in atmospheric transport-chemistry models, *Atmos. Environ.*, 27A, 2591–2611, 1993. 5855
- Hicks, B. B., Hosker, R. P., Myers, T. P., and Womack, J. D.: Dry deposition measurement techniques, I, Design and tests of a prototype meteorological and chemical system for determining dry deposition, *Atmos. Environ.*, 25, 2345–2359, 1991. 5818
- 25 Hintsä, E. J., Boering, K. A., Weinstock, E. M., Anderson, J. G., Gary, B. L., Pfister, L., Daube, B. C., Wofsy, S. C., Loewenstein, M., Podolske, J. R., Margitan, J. J., and Bui, T. P.: Troposphere-to-stratosphere transport in the lowermost stratosphere from measurements of H<sub>2</sub>O, CO<sub>2</sub>, N<sub>2</sub>O and O<sub>3</sub>, *Geophys. Res. Lett.*, 25(14), 2655–2658, doi:10.1029/98GL01797, 1998. 5830
- 30 Houghton, J. T., Ding, Y., Griggs, D. J., Noguera, M., van der Linden, P. J., Dai, X., Maskell, K., and Johnson, C. A.: Chapt. 4: Atmospheric chemistry and greenhouse gases, in: *Climate Change 2001: The Scientific Basis, Contribution of Working Group I to the Third Assessment Report of the Intergovernmental Panel on Climate Change*, edited by: Houghton, J. T., Ding,

**Hydrogen isotope  
modelling**

G. Pieterse et al.

Title Page

Abstract

Introduction

Conclusions

References

Tables

Figures

◀

▶

◀

▶

Back

Close

Full Screen / Esc

Printer-friendly Version

Interactive Discussion



Y., Griggs, D. J., Noguera, M., van der Linden, P. J., Dai, X., Maskell, K., and Johnson, C. A., Cambridge University Press, Cambridge, UK and New York, NY, USA, 2001. 5835

Houweling, S., Dentener, F., and Lelieveld, J.: The impact of non-methane hydrocarbon compounds on tropospheric photochemistry, *J. Geophys. Res.*, 103(D9), 10673–10696, 1998. 5815, 5835

Krol, M., Houweling, S., Bregman, B., van den Broek, M., Segers, A., van Velthoven, P., Peters, W., Dentener, F., and Bergamaschi, P.: The two-way nested global chemistry-transport zoom model TM5: algorithm and applications, *Atmos. Chem. Phys.*, 5, 417–432, doi:10.5194/acp-5-417-2005, 2005. 5814, 5815

Lelieveld, J., Bregman, B., Arnold, F., Bürger, V., Crutzen, P. J., Fischer, H., Waibel, A., Siegmund, P., and van Velthoven, P. F. J.: Chemical perturbation of the lowermost stratosphere through exchange with the troposphere, *Geophys. Res. Lett.*, 24(5), 603–606, doi:10.1029/97GL00255, 1997. 5830

Leone, J. A. and Seinfeld, J. H.: Comparative analysis of chemical reaction mechanisms for photochemical smog, *Atmos. Environ.*, 19, 437–464, 1985. 5855

McCarthy, M. C., Boering, K. A., Rahn, T., Eiler, J., Rice, A., Tyler, S. C., and Atlas, E.: The hydrogen isotopic composition of water vapor entering the stratosphere inferred from high precision measurements of  $\delta D-CH_4$  and  $\delta D-H_2$ , *J. Geophys. Res.*, 109, D07304, doi:10.1029/2003JD004003, 2004. 5816, 5817, 5834

McCaulley, J. A., Kelly, N., Golde, M. F., and Kaufman, F.: Kinetic studies of the reactions of F and OH with  $CH_3OH$ , *J. Phys. Chem.*, 93, 1014–1018, 1989. 5839

Meirink, J. F., Bergamaschi, P., Frankenberg, C., d'Amelio, M. T. S., Dlugokencky, E. J., Gatti, L. V., Houweling, S., Miller, J. B., Röckmann, T., Villani, M. G., and Krol, M. C.: Four-dimensional variational data assimilation for inverse modelling of atmospheric methane emissions: Analysis of SCIAMACHY observations, *J. Geophys. Res.*, 113, D17301, doi:10.1029/2007JD009740, 2008a. 5817, 5835

Meirink, J. F., Bergamaschi, P., and Krol, M. C.: Four-dimensional variational data assimilation for inverse modelling of atmospheric methane emissions: method and comparison with synthesis inversion, *Atmos. Chem. Phys.*, 8, 6341–6353, doi:10.5194/acp-8-6341-2008, 2008b. 5817, 5835

Meyers, T. P., Finkelstein, P., Clarke, J., Ellestad, T. G., and Sims, P. F.: A multilayer model for inferring dry deposition using standard meteorological measurements, *J. Geophys. Res.*, 103(D17), 22645–22661, 1998. 5819

Moortgat, G. K., Klippel, W., Mobius, K. H., Seiler, W., and Warneck, P.: MPIC two dimensional model, Technical Report Rep. FAA-EE-80-47, US Dept. of Transp., Washington, DC, USA, 1980. 5853

5 Nilsson, E. J. K., Johnson, M. S., Taketani, F., Matsumi, Y., Hurley, M. D., and Wallington, T. J.: Atmospheric deuterium fractionation: HCHO and HCDO yields in the  $\text{CH}_2\text{DO} + \text{O}_2$  reaction, *Atmos. Chem. Phys.*, 7, 5873–5881, doi:10.5194/acp-7-5873-2007, 2007. 5813, 5814, 5836

10 Nilsson, E. J. K., Andersen, V. F., Skov, H., and Johnson, M. S.: Pressure dependent deuterium fractionation in the formation of molecular hydrogen in formaldehyde photolysis, *Atmos. Chem. Phys. Discuss.*, 9, 24029–24050, doi:10.5194/acpd-9-24029-2009, 2009. 5813, 5814, 5838, 5853

15 van Noije, T. P. C., Eskes, H. J., van Weele, M., and van Velthoven, P. F. J.: Implications of the enhanced Brewer-Dobson circulation in European Centre for Medium-Range Weather Forecasts reanalysis ERA-40 for the stratosphere-troposphere exchange of ozone in global chemistry transport models, *J. Geophys. Res.*, 109, D19308, doi:10.1029/2004JD004586, 2004. 5831

20 van Noije, T. P. C., Segers, A. J., and van Velthoven, P. F. J.: Time series of the stratosphere-troposphere exchange of ozone simulated with reanalyzed and operational forecast data, *J. Geophys. Res.*, 111, D03301, doi:10.1029/2005JD006081, 2006. 5831

25 Novelli, P. C., Lang, P. M., Masarie, K. A., Hurst, D. F., Myers, R., and Elkins, J. W.: Molecular hydrogen in the troposphere: Global distribution and budget, *J. Geophys. Res.*, 104, 30427–30444, 1999. 5813, 5815, 5818, 5827, 5850

Olivier, J. G. J. and Berdowski, J. J. M.: Global emissions sources and sinks, in: *The Climate System*, edited by: Berdowski, J., Guicherit, R., and Heij, B. J., A.A. Balkema Publishers/Swets & Zeitlinger Publishers, Lisse, The Netherlands, 2001. 5817

30 Pieterse, G., Krol, M. C., and Röckmann, T.: A consistent molecular hydrogen isotope chemistry scheme based on an independent bond approximation, *Atmos. Chem. Phys.*, 9, 8503–8529, doi:10.5194/acp-9-8503-2009, 2009. 5814, 5815, 5816, 5829, 5836, 5837, 5838, 5839, 5853, 5854

Price, H., Jaeglé, L., Rice, A., Quay, P., Novelli, P. C., and Gammon, R.: Global budget of molecular hydrogen and its deuterium content: constraints from ground station, cruise, and aircraft observations, *J. Geophys. Res.*, 112, D22108, doi:10.1029/2006JD008152, 2007. 5813, 5814, 5818, 5823, 5826, 5827, 5831, 5834

Quay, P., Stutsman, J., Wilbur, D., Snover, A., Dlugokencky, E., and Brown, T.: The isotopic

ACPD

11, 5811–5866, 2011

## Hydrogen isotope modelling

G. Pieterse et al.

Title Page

Abstract

Introduction

Conclusions

References

Tables

Figures

◀

▶

◀

▶

Back

Close

Full Screen / Esc

Printer-friendly Version

Interactive Discussion



- composition of atmospheric methane, *Global Biogeochem. Cy.*, 13, 445–461, 1999. 5835
- Rahn, T., Eiler, J. M., Kitchen, N., Fessenden, J. E., and Randerson, J. T.: Concentration and  $\delta D$  of molecular hydrogen in boreal forests: ecosystem-scale systematics of atmospheric  $H_2$ , *Geophys. Res. Lett.*, 1888, 29, doi:10.1029/2002GL015118, 2002a. 5814
- 5 Rahn, T., Kitchen, N., and Eiler, J. M.: D/H ratios of atmospheric  $H_2$  in urban air: results using new methods for analysis of nano-molar  $H_2$  samples, *Geochim. Cosmochim. Ac.*, 66, 2475–2481, 2002b. 5814, 5827
- Rahn, T., Eiler, J. M., Boering, K. A., Wennberg, P. O., McCarthy, M. C., Tyler, S., Schauffler, S., Donnelly, S., and Atlas, E.: Extreme deuterium enrichment in stratospheric hydrogen and the global atmospheric budget of  $H_2$ , *Nature*, 424, 918–921, 2003. 5813, 5814, 5830, 5832
- 10 Ravishankara, A. R.: Kinetics of radical reactions in the atmospheric oxidation of  $CH_4$ , *Annu. Rev. Phys. Chem.*, 39, 367–394, 1988. 5836
- Rayleigh, L.: On the distillation of binary mixtures, *Philos. Mag.*, 4(23), 521–537, 1902. 5826
- Reid, S. J. and Vaughan, G.: Lamination in ozone profiles in the lower stratosphere, *Q. J. Roy. Meteorol. Soc.*, 117, 825–844, 1991. 5830
- 15 Rhee, T. S., Brenninkmeijer, C. A. M., and Röckmann, T.: The overwhelming role of soils in the global atmospheric hydrogen cycle, *Atmos. Chem. Phys.*, 6, 1611–1625, doi:10.5194/acp-6-1611-2006, 2006. 5813, 5818, 5827
- Rhee, T. S., Brenninkmeijer, C. A. M., and Röckmann, T.: Hydrogen isotope fractionation in the photolysis of formaldehyde, *Atmos. Chem. Phys.*, 8, 1353–1366, doi:10.5194/acp-8-1353-2008, 2008. 5813, 5814, 5838, 5839
- 20 Rice, A., Quay, P., Stutsman, J., Gammon, R., Price, H., and Jaeglé, L.: Meridional distribution of molecular hydrogen and its deuterium content in the atmosphere, *J. Geophys. Res.*, 115, D12306, doi:10.1029/2009JD012529, 2010. 5815, 5821, 5858
- 25 Roberts, J. M. and Fayer, R. W.: UV absorption cross section of organic nitrates of potential atmospheric importance and estimation of atmospheric lifetimes, *Environ. Sci. Technol.*, 23, 945–951, 1989. 5855
- Röckmann, T., Rhee, T. S., and Engel, A.: Heavy hydrogen in the stratosphere, *Atmos. Chem. Phys.*, 3, 2015–2023, doi:10.5194/acp-3-2015-2003, 2003. 5813, 5830
- 30 Röckmann, T., Walter, S., Bohn, B., Wegener, R., Spahn, H., Brauers, T., Tillmann, R., Schlosser, E., Koppmann, R., and Rohrer, F.: Isotope effect in the formation of  $H_2$  from  $H_2CO$  studied at the atmospheric simulation chamber SAPHIR, *Atmos. Chem. Phys.*, 10, 5343–5357, doi:10.5194/acp-10-5343-2010, 2010. 5813, 5814, 5838, 5853

**Hydrogen isotope  
modelling**

G. Pieterse et al.

Title Page

Abstract

Introduction

Conclusions

References

Tables

Figures

◀

▶

◀

▶

Back

Close

Full Screen / Esc

Printer-friendly Version

Interactive Discussion



- Sander, S. P., Finlayson-Pitts, B. J., Friedl, R. R., Golden, D. M., Huie, R. E., Keller-Rudek, H., Kolb, C. E., Kurylo, M. J., Molina, M. J., Moortgat, G. K., Orkin, V. L., R., R. A., and Wine, P. H.: Chemical Kinetics and Photochemical Data for Use in Atmospheric Studies, Evaluation Number 15, Technical Report, JPL Publication 06-2, Jet Propulsion Laboratory, Pasadena, 2006. 5836, 5837, 5853, 5854
- Sanderson, M. G., Collins, W. J., Derwent, R. G., and Johnson, C. E.: Simulation of global hydrogen levels using a lagrangian three dimensional model, *J. Atmos. Chem.*, 46, 15–28, 2003. 5813, 5818
- Schmidt, H. L., Werner, R. A., and Eisenreich, W. (2003): Systematics of  $^2\text{H}$  patterns in natural compounds and its importance for the elucidation of biosynthetic pathways, *Phytochem. Rev.*, 2, 61–85, 2003. 5816
- Schultz, M. and Stein, O.: GEMS (GRG) emissions for 2003 reanalysis simulations, Technical report, MPI-M, Max Planck Institute for Meteorology, Hamburg, Germany, 2006. 5818
- Schultz, M. G., Diehl, T., Brasseur, G. P., and Zittel, W.: Air pollution and climate-forcing impacts of a global hydrogen economy, *Science*, 302, 624–627, 2003. 5813
- Seiler, W. and Conrad, R.: Contribution of tropical ecosystems to the global budgets for trace gases, especially  $\text{CH}_4$ ,  $\text{H}_2$ ,  $\text{CO}$  and  $\text{N}_2\text{O}$ , in: *The Geophysiology of Amazonia: Vegetation and Climate Interactions*, edited by: Dickerson, R., John Wiley, New York, 33–62, 1987. 5813
- Senum, G. I., Lee, Y. N., and Gaffney, J. S.: Ultraviolet absorption spectrum of peroxy acetyl nitrate and peroxy propionyl nitrate, *J. Phys. Chem.*, 88, 1269–1270, 1984. 5855
- Stockwell, W. R., Kirchner, F., Kuhn, M., and Seefeld, S.: A new mechanism for regional atmospheric chemistry modeling, *J. Geophys. Res.*, 102, 25847–25879, 1997. 5855
- Tromp, T. K., Shia, R.-L., Allen, M., Eiler, J. M., and Yung, Y. L.: Potential environmental impact of a hydrogen economy on the stratosphere, *Science*, 300, 1740–1742, 2003. 5813
- Vollmer, M. K., Walter, S., Bond, S. W., Soltic, P., and Röckmann, T.: Molecular hydrogen ( $\text{H}_2$ ) emissions and their isotopic signatures (H/D) from a motor vehicle: implications on atmospheric  $\text{H}_2$ , *Atmos. Chem. Phys.*, 10, 5707–5718, doi:10.5194/acp-10-5707-2010, 2010. 5814, 5832
- Warneck, P.: *Chemistry of the natural atmosphere*, Int. Geophys. Ser., Academic, San Diego, Calif., 757 pp., 1988. 5813
- Warwick, N. J., Bekki, S., Nisbet, E. G., and Pyle, J. A.: Impact of a hydrogen economy on the stratosphere and troposphere studied in a 2-D model, *Geophys. Res. Lett.*, 31, L05107, doi:10.1029/2003GL019224, 2004. 5813

**Hydrogen isotope  
modelling**

G. Pieterse et al.

Title Page

Abstract

Introduction

Conclusions

References

Tables

Figures

◀

▶

◀

▶

Back

Close

Full Screen / Esc

Printer-friendly Version

Interactive Discussion



Wille, U., Becker, E., Schindler, R. N., Lancer, I. T., Poulet, G., and LeBras, G.: A discharge flow mass-spectrometric study of the reaction of the NO<sub>3</sub> radical and isoprene, *J. Atmos. Chem.*, 13, 183–193, 1991. 5855

5 Xiao, X., Prinn, R. G., Simmonds, P. G., Steele, L. P., Novelli, P. C., Huang, J., Langenfelds, R. L., O'Doherty, S., Krummel, P. B., Fraser, P. J., Porter, L. W., Weiss, R. F., Salameh, P., and Wang, R. H. J.: Optimal estimation of the soil uptake of molecular hydrogen from the advanced global atmospheric gases experiments and other measurements, *J. Geophys. Res.*, 112, D07303, doi:10.1029/2006JD007241, 2007. 5815, 5818

10 Yonemura, S., Kawashima, S., and Tsuruta, H.: Carbon monoxide, hydrogen, and methane uptake by soils in a temperate arable field and a forest, *J. Geophys. Res.*, 105(D11), 14347–14362, 2000. 5818

## Hydrogen isotope modelling

G. Pieterse et al.

Title Page

Abstract

Introduction

Conclusions

References

Tables

Figures

◀

▶

◀

▶

Back

Close

Full Screen / Esc

Printer-friendly Version

Interactive Discussion



**Table 1.** Global budget of H<sub>2</sub> in Tg H<sub>2</sub> per year.

	Novelli et al. (1999)	Hauglustaine and Ehhalt (2002)	Sanderson et al. (2003)	Rhee et al. (2006)	Price et al. (2007)	Xiao et al. (2007)	Ehhalt and Rohrer (2009)	This work
<b>Sources</b>								
Fossil fuel	15	16	20.0	15	18.3	15	11	17.0 <sup>+3</sup> <sub>-6</sub>
Biomass burning	16	13	20.0	16	10.1	13	15	15.0 <sup>+5</sup> <sub>-5</sub>
Biofuel					4.4			
Ocean N <sub>2</sub> fixation	3	5	4.0	6	6.0		6	5.0 <sup>+1</sup> <sub>-0.6</sub>
Land N <sub>2</sub> fixation	3	5	4.0	6	0.0		3	3.0 <sup>+0.6</sup> <sub>-0.3</sub>
Photochemical production	40	31	30.2	64	34.3	77	41	37.3
Total	77	70	78.2	107	73.1	105	76	77.3
<b>Sinks</b>								
Photochemical removal	19	15	17.1	19	18.0	18	19	22.1
Deposition	56	55	58.3	88	55.0	85	60	55.8
Total	75	70	75.4	107	73.0	105 <sup>a</sup>	79	77.9
Tropospheric burden (Tg H <sub>2</sub> )	155	136	172 <sup>b</sup>	150 <sup>c</sup>	141	149	155 <sup>d</sup>	169 <sup>e</sup>
Tropospheric lifetime (yr)	2.1	1.9	2.2 <sup>b</sup>	1.4	1.9	1.4	2.0	2.2 <sup>e</sup>

<sup>a</sup> Includes export to stratosphere of 1.9 Tg H<sub>2</sub> per year.

<sup>b</sup> The model domain for the budget calculation reached 100 hPa. For the troposphere with a mass of 0.82 of the total atmosphere the burden would be 157 Tg H<sub>2</sub> and the tropospheric lifetime 2.0 yr.

<sup>c</sup> Calculated from sources and lifetime.

<sup>d</sup> From Novelli et al. (1999).

<sup>e</sup> The model domain for the budget calculation runs from the surface to 100 hPa. For the troposphere with a mass of 0.82 of the total atmosphere the burden would be 155 Tg H<sub>2</sub> and the lifetime 2.0 yr.

Title Page

Abstract

Introduction

Conclusions

References

Tables

Figures

◀

▶

◀

▶

Back

Close

Full Screen / Esc

Printer-friendly Version

Interactive Discussion



Hydrogen isotope  
modelling

G. Pieterse et al.

Title Page

Abstract

Introduction

Conclusions

References

Tables

Figures

◀

▶

◀

▶

Back

Close

Full Screen / Esc

Printer-friendly Version

Interactive Discussion

**Table 2.** Global isotope budget of H<sub>2</sub> up to 100 mbar.

	Magnitude (Tg H <sub>2</sub> /yr)	Signature <sup>a</sup>	Relative signature <sup>b</sup>	Composition (‰)
<b>Sources</b>				
Fossil fuel	17.0 <sup>+3</sup> <sub>-6</sub>	-196	2.754 × 10 <sup>-5</sup>	
Biomass burning	15.0 <sup>+5</sup> <sub>-5</sub>	-260	2.237 × 10 <sup>-5</sup>	
Ocean N <sub>2</sub> fixation	5.0 <sup>+1</sup> <sub>-2</sub>	-628	3.748 × 10 <sup>-6</sup>	
Land N <sub>2</sub> fixation	3.0 <sup>+3</sup> <sub>-3</sub>	-628	2.249 × 10 <sup>-6</sup>	
Photochemical production	37.3	+116	8.391 × 10 <sup>-5</sup>	
Total	77.3		1.398 × 10 <sup>-4</sup>	
<b>Sinks</b>				
Photochemical removal	22.1	0.542 <sup>c</sup>	0.154	
Deposition	55.8	0.925 <sup>c</sup>	0.663	
Total	77.9		0.817	
<b>Isotopic composition</b>				
From budget				99
Modelled composition				128
Stratospheric contribution				29

<sup>a</sup> Sources are expressed in ‰, sinks are expressed in fractionation constants.<sup>b</sup> Source or sink signature weighted by the flux magnitude.<sup>c</sup> Calculated by Eq. (7).

Hydrogen isotope  
modelling

G. Pieterse et al.

**Table 3.** Sensitivity of isotopic composition of H<sub>2</sub> on changes in scheme variables.

Scenario	Perturbed variables	Composition (‰)
Default <sup>a</sup>		+128
1a	KIE[R32b] = 1.100, KIE[R33b] = 1.820	+82
1b	$KIE[R33b] = (500.00 + 2.50 \times 10^{-2} p) / (500.00 + 1.60 \times 10^{-2} p)$	+146
2a	Stratospheric composition increased by 20‰	+140
2b	Tropopause boundary defined by $p_s = 2.10 \times 10^4 - 1.65 \times 10^4 \cos(\theta)$	+116
2c	Tropopause boundary defined by $p_s = 2.00 \times 10^4 - 1.15 \times 10^4 \cos(\theta)$	+118
3	$\delta D[NMHCs] = -200\%$	+118
4a	$\delta D[N_2 \text{ fixation emissions}] = -700\%$	+124
4b	$\delta D[\text{fossil fuel burning emissions}] = -250\%$	+123
4c	$\delta D[\text{biomass burning emissions}] = -290\%$	+125
5	Fractionation constant deposition changed to 0.900	+142

<sup>a</sup> The default scenario uses KIE[R32b] = 1.580, KIE[R33b] =  $(500.00 + 2.50 \times 10^{-2} p) / (500.00 + 1.34 \times 10^{-2} p)$ , a tropopause composition of +130‰, a tropopause boundary defined by  $p_s = 3.00 \times 10^4 - 2.15 \times 10^4 \cos(\theta)$ ,  $\delta D[NMHCs] = -86\%$ ,  $\delta D[N_2 \text{ fixation emissions}] = -628\%$ ,  $\delta D[\text{fossil fuel burning emissions}] = -196\%$ ,  $\delta D[\text{biomass burning emissions}] = -260\%$ , and fractionation constant of 0.943 for deposition.

Title Page

Abstract

Introduction

Conclusions

References

Tables

Figures

◀

▶

◀

▶

Back

Close

Full Screen / Esc

Printer-friendly Version

Interactive Discussion



**Table A1.** Overview of modified CBM-4 reactions related to methane and molecular hydrogen chemistry.

Number	Reaction	A	–E/R	<i>n</i>	KIE	Reference
R21a	H <sub>2</sub> + OH → HO <sub>2</sub>	2.8 × 10 <sup>–12</sup>	–1800			JPL06
R21b	HD + OH → <sup>a</sup>	5.0 × 10 <sup>–12</sup>	–2130			JPL06
R26a	CH <sub>4</sub> + OH → CH <sub>3</sub> OO	2.45 × 10 <sup>–12</sup>	–1775			JPL06
R26b	CH <sub>3</sub> D + OH → α <sub>CH<sub>3</sub>D+OH</sub> <sup>DC<sub>H<sub>3</sub>D+OH</sub></sup>	3.50 × 10 <sup>–12</sup>	–1950			JPL06
R27a	CH <sub>3</sub> OO + NO → CH <sub>2</sub> O + HO <sub>2</sub> + NO <sub>2</sub>	4.2 × 10 <sup>–12</sup>	180			JPL
R27b	CH <sub>2</sub> DOO + NO → 0.882CHDO <sup>a</sup>				1.323	GP
R28a	CH <sub>3</sub> OO + HO <sub>2</sub> → CH <sub>3</sub> OOH	3.8 × 10 <sup>–13</sup>	800			JPL
R28b	CH <sub>2</sub> DOO + HO <sub>2</sub> → CH <sub>2</sub> DOOH				1.000	GP
R29a	CH <sub>3</sub> OO + CH <sub>3</sub> OO → 2.000CH <sub>2</sub> O + 0.667HO <sub>2</sub>	2.5 × 10 <sup>–13</sup>	190			JPL
R29b	CH <sub>2</sub> DOO + CH <sub>3</sub> OO → 0.810CHDO <sup>a</sup>				1.221	<sup>b</sup>
R30a	CH <sub>3</sub> OOH + OH → 0.700CH <sub>3</sub> OO + 0.300CH <sub>2</sub> O + 0.300OH	3.8 × 10 <sup>–12</sup>	200			JPL
R30b	CH <sub>2</sub> DOOH + OH → 0.755CH <sub>2</sub> DOO + 0.216CHDO <sup>a</sup>				1.079	GP
R31a	CH <sub>3</sub> OOH $\xrightarrow{h\nu}$ CH <sub>2</sub> O + HO <sub>2</sub> + OH					BC
R31b	CH <sub>2</sub> DOOH $\xrightarrow{h\nu}$ 0.882CHDO <sup>a</sup>				1.323	GP
R32a	CH <sub>2</sub> O $\xrightarrow{h\nu}$ 2HO <sub>2</sub> + CO					BC
R32b	CHDO $\xrightarrow{h\nu}$ <sup>a</sup>				1.580	BC
R33a	CH <sub>2</sub> O $\xrightarrow{h\nu}$ CO + H <sub>2</sub>					MO
R33b	CHDO $\xrightarrow{h\nu}$ CO + HD				<sup>c</sup>	
R34a	CH <sub>2</sub> O + OH → HO <sub>2</sub> + CO	5.5 × 10 <sup>–12</sup>	125			JPL06
R34b	CHDO + OH → <sup>a</sup>				1.280	<sup>d</sup>
R35a	CH <sub>2</sub> O + NO <sub>3</sub> → HNO <sub>3</sub> + HO <sub>2</sub> + CO	5.8 × 10 <sup>–16</sup>				AT1
R35b	CHDO + NO <sub>3</sub> → <sup>a</sup>				1.000	<sup>e</sup>

In this table, the rate constants are in molec<sup>*p*</sup> cm<sup>–*q*</sup> s<sup>–1</sup>, with *p* and *q* reaction molecularity dependent. Photolysis rates are wavelength and intensity dependent (see references). CO<sub>2</sub>, O<sub>2</sub> and H<sub>2</sub>O are not listed in reaction products. BC, Brühl and Crutzen (1992); GP, Pieterse et al. (2009); JPL, DeMore et al. (1994); JPL06, Sander et al. (2006); MO, Moortgat et al. (1980); AT, Atkinson et al. (1992).

<sup>a</sup> The production of the deuterium free radical species is neglected because of the small amount of the deuterium containing precursor compared to the deuterium free precursor.

<sup>b</sup> Derived in Sect. A2.

<sup>c</sup> Here KIE = (500.00 + 2.50 × 10<sup>–2</sup>*p*)/(500.00 + 1.34 × 10<sup>–2</sup>*p*), where *p* is the ambient pressure in Pa (Nilsson et al., 2009; Röckmann et al., 2010).

<sup>d</sup> Derived in Sect. A4.

<sup>e</sup> Because this term is of little importance for the H<sub>2</sub> budget, isotope effects are not considered here.

## Hydrogen isotope modelling

G. Pieterse et al.

Title Page

Abstract

Introduction

Conclusions

References

Tables

Figures

◀

▶

◀

▶

Back

Close

Full Screen / Esc

Printer-friendly Version

Interactive Discussion



**Table A2.** Reactions following the CH<sub>3</sub>OO self reaction (Sander et al., 2006; Pieterse et al., 2009).

Number	Reaction	IB ratio		KIE
B1a <sub>1</sub>	CH <sub>3</sub> OO + CH <sub>3</sub> OO	$\xrightarrow{0.333}$	2CH <sub>3</sub> O + O <sub>2</sub>	
B1a <sub>2</sub>		$\xrightarrow{0.667}$	CH <sub>3</sub> OH + CH <sub>2</sub> O + O <sub>2</sub>	
B1b <sub>1</sub>	CH <sub>2</sub> DOO + CH <sub>3</sub> OO	$\xrightarrow{0.333}$	CH <sub>2</sub> DO + CH <sub>3</sub> O + O <sub>2</sub>	1.000
B1b <sub>2</sub>		$\xrightarrow{0.334}$	CH <sub>2</sub> DOH + CH <sub>2</sub> O + O <sub>2</sub>	1.000
B1b <sub>3</sub>		$\xrightarrow{0.222}$	CH <sub>3</sub> OH + CHDO + O <sub>2</sub>	1.000
B1b <sub>4</sub>		$\xrightarrow{0.111}$	CH <sub>3</sub> OD + CH <sub>2</sub> O + O <sub>2</sub>	1.000
B2a <sub>1</sub>	CH <sub>3</sub> OH + O <sub>2</sub>	$\xrightarrow{0.150}$	CH <sub>3</sub> O + H <sub>2</sub> O	
B2a <sub>2</sub>		$\xrightarrow{0.850}$	CH <sub>2</sub> OH + H <sub>2</sub> O	
B2b <sub>1</sub>	CH <sub>2</sub> DOH + OH	$\xrightarrow{0.189}$	CH <sub>2</sub> DO + H <sub>2</sub> O	1.262
B2b <sub>2</sub>		$\xrightarrow{0.715}$	CHDOH + H <sub>2</sub> O	1.262
B2b <sub>3</sub>		$\xrightarrow{0.096}$	CH <sub>2</sub> OH + HDO	1.262
B2c <sub>1</sub>	CH <sub>3</sub> OD + OH	$\xrightarrow{1.000}$	CH <sub>2</sub> OD + H <sub>2</sub> O	1.176
B2c <sub>2</sub>		$\xrightarrow{0.000}$	CH <sub>3</sub> O + HDO	1.176
B3a	CH <sub>2</sub> OH + O <sub>2</sub>	$\xrightarrow{1.000}$	CH <sub>2</sub> O + HO <sub>2</sub>	
B3b	CH <sub>2</sub> OD + O <sub>2</sub>	$\xrightarrow{1.000}$	CH <sub>2</sub> O + DO <sub>2</sub>	1.000
B3c	CHDOH + O <sub>2</sub>	$\xrightarrow{1.000}$	CHDO + HO <sub>2</sub>	1.000
B4a	CH <sub>3</sub> O + O <sub>2</sub>	$\xrightarrow{1.000}$	CH <sub>2</sub> O + HO <sub>2</sub>	
B4b <sub>1</sub>	CH <sub>2</sub> DO + O <sub>2</sub>	$\xrightarrow{0.882}$	CHDO + HO <sub>2</sub>	1.323
B4b <sub>2</sub>		$\xrightarrow{0.118}$	CH <sub>2</sub> O + DO <sub>2</sub>	1.323

Hydrogen isotope  
modelling

G. Pieterse et al.

Title Page

Abstract

Introduction

Conclusions

References

Tables

Figures

◀

▶

◀

▶

Back

Close

Full Screen / Esc

Printer-friendly Version

Interactive Discussion



**Table B1.** Overview of modified CBM-IV NMHC reactions.

Number	Reaction	A	-E/R	n	KIE	Reference
R37	ALD2 + OH → HO <sub>2</sub>	7.0 × 10 <sup>-12</sup>	250			G1
R38a	ALD2 + NO <sub>3</sub> → C <sub>2</sub> O <sub>3</sub> + HNO <sub>3</sub>	2.5 × 10 <sup>-15</sup>				G1
R38b	ALD2(D) + NO <sub>3</sub> → a <sup>a</sup>				1.000 <sup>b</sup>	
R39a	ALD2 $\xrightarrow{h\nu}$ CH <sub>2</sub> O + XO <sub>2</sub> + CO + 2HO <sub>2</sub>					LS
R39b	ALD2(D) $\xrightarrow{h\nu}$ CHDO <sup>c</sup>				1.000 <sup>b</sup>	
R40a	C <sub>2</sub> O <sub>3</sub> + NO → CH <sub>2</sub> O <sub>2</sub> + NO <sub>2</sub>	3.5 × 10 <sup>-11</sup>	-180			G2
R40b	C <sub>2</sub> O <sub>3</sub> (D) + NO → CH <sub>2</sub> DO <sub>2</sub> (D) <sup>c</sup>				1.000 <sup>b</sup>	
R41	C <sub>2</sub> O <sub>3</sub> + NO <sub>2</sub> $\xrightarrow{M}$ PAN	k <sub>0</sub> 2.6 × 10 <sup>-28</sup> k <sub>∞</sub> 1.2 × 10 <sup>-11</sup> 2.0 × 10 <sup>-18</sup>		-7.1 0.9		ATG
R42	PAN → C <sub>2</sub> O <sub>3</sub> + NO <sub>2</sub>		-13500			G2
R43	PAN $\xrightarrow{h\nu}$ C <sub>2</sub> O <sub>3</sub> + NO <sub>2</sub>					SEN
R44a	C <sub>2</sub> O <sub>3</sub> + C <sub>2</sub> O <sub>3</sub> → 2CH <sub>3</sub> O <sub>2</sub>	2.0 × 10 <sup>-12</sup>				G1
R44b	C <sub>2</sub> O <sub>3</sub> + C <sub>2</sub> O <sub>3</sub> (D) → CH <sub>2</sub> O <sub>2</sub> + CH <sub>2</sub> DO <sub>2</sub>				1.000 <sup>b</sup>	
R45a	C <sub>2</sub> O <sub>3</sub> + HO <sub>2</sub> → CH <sub>2</sub> O <sub>2</sub> + 0.79OH + 0.21ROOH	6.5 × 10 <sup>-12</sup>				G1
R45b	C <sub>2</sub> O <sub>3</sub> (D) + HO <sub>2</sub> → CH <sub>2</sub> DO <sub>2</sub> <sup>c</sup>				1.000 <sup>b</sup>	
R46	PAR + OH → 0.87XO <sub>2</sub> + 0.76ROR + 0.13XO <sub>2</sub> N + 0.11HO <sub>2</sub> + 0.11ALD2 + 0.11RXPAR	8.1 × 10 <sup>-13</sup>				G1
R47	ROR → 1.10ALD2 + 0.96XO <sub>2</sub> + 0.94HO <sub>2</sub> + 2.10RXPAR	1.0 × 10 <sup>-15</sup>	-8000			G1
R48	ROR → HO <sub>2</sub>	1.6 × 10 <sup>3</sup>				G1
R49a	OLE + OH → CH <sub>2</sub> O + ALD2 + XO <sub>2</sub> + HO <sub>2</sub> + RXPAR	5.2 × 10 <sup>-12</sup>	504			G1
R49b	OLE(D) + OH → 0.500CHDO <sup>c</sup>				1.000 <sup>b</sup>	
R50a	OLE + O <sub>3</sub> → 0.44ALD2 + 0.64CH <sub>2</sub> O + 0.37CO + 0.25HO <sub>2</sub> + 0.29XO <sub>2</sub> + 0.40OH + 0.90RXPAR	4.33 × 10 <sup>-15</sup>	-1800			STO
R50b	OLE(D) + O <sub>3</sub> → 0.320CHDO <sup>c</sup>				1.000 <sup>b</sup>	
R51a	OLE + NO <sub>3</sub> → 0.91XO <sub>2</sub> + CH <sub>2</sub> O + ALD2 + 0.09XO <sub>2</sub> N + NO <sub>2</sub> + RXPAR	7.7 × 10 <sup>-15</sup>				G1
R51b	OLE(D) + NO <sub>3</sub> → 0.320CHDO <sup>c</sup>				1.000 <sup>b</sup>	
R52a	ETH + OH $\xrightarrow{M}$ XO <sub>2</sub> + HO <sub>2</sub> + 1.56CH <sub>2</sub> O + 0.22ALD2	k <sub>0</sub> 1.0 × 10 <sup>-28</sup> k <sub>∞</sub> 8.8 × 10 <sup>-12</sup>		0.8 0.0		JPL
R52b	ETH(D) + OH → 0.780CHDO <sup>c</sup>				1.000 <sup>b</sup>	
R53a	ETH + O <sub>3</sub> → CH <sub>2</sub> O + 0.43CO + 0.26HO <sub>2</sub> + 0.12OH	9.1 × 10 <sup>-15</sup>	-2580			JPL
R53b	ETH(D) + O <sub>3</sub> → 0.500CHDO <sup>c</sup>				1.000 <sup>b</sup>	
R54	MGLY + OH → XO <sub>2</sub> + C <sub>2</sub> O <sub>3</sub>	1.7 × 10 <sup>-11</sup>				AT1
R55	MGLY $\xrightarrow{h\nu}$ C <sub>2</sub> O <sub>3</sub> + HO <sub>2</sub> + CO					G1
R56a	ISOP + OH → 0.85XO <sub>2</sub> + 0.61CH <sub>2</sub> O + 0.85HO <sub>2</sub> + 0.03MGLY + 0.58OLE + 0.15XO <sub>2</sub> N + 0.63PAR	2.54 × 10 <sup>-11</sup>	410			AT1
R56b	ISOP(D) + OH → 0.305CHDO <sup>c</sup>				1.000 <sup>b</sup>	
R57a	ISOP + O <sub>3</sub> → 0.90CH <sub>2</sub> O + 0.55OLE + 0.18XO <sub>2</sub> + 0.36CO + 0.15C <sub>2</sub> O <sub>3</sub> + 0.03MGLY + 0.63PAR + 0.30HO <sub>2</sub> + 0.28OH	1.23 × 10 <sup>-14</sup>	-2013			AT1
R57b	ISOP(D) + O <sub>3</sub> → 0.450CHDO <sup>c</sup>				1.000 <sup>b</sup>	
R58a	ISOP + NO <sub>3</sub> → 0.90HO <sub>2</sub> + 0.90ORGNIT + 0.03CH <sub>2</sub> O + 0.45OLE + 0.12ALD + 0.10NO <sub>2</sub> + 0.08MGLY	7.8 × 10 <sup>-13</sup>				WL
R58b	ISOP(D) + NO <sub>3</sub> → 0.015CHDO <sup>c</sup>				1.000 <sup>b</sup>	

In this table, the rate constants are in molec<sup>p</sup> cm<sup>-q</sup> s<sup>-1</sup>, with *p* and *q* reaction molecularity dependent. Photolysis rates are wavelength and intensity dependent (see references). CO<sub>2</sub>, O<sub>2</sub> and H<sub>2</sub>O are not listed in reaction products. G1, Gery et al. (1989); G2, Gery et al. (1988); JPL, DeMore et al. (1994); LS, Leone and Seinfeld (1985); SEN, Senum et al. (1984); AT1, Atkinson (1994); WL, Wille et al. (1991); RF, Roberts and Fayer (1989); HT, Hertel et al. (1993); STO, Stockwell et al. (1997); ATG, based on Atkinson (1994) and Gery et al. (1989).

<sup>a</sup> Here the production of HNO<sub>3</sub> is neglected because the small amount of ALD2(D) involved. Actually, C<sub>2</sub>O<sub>3</sub>(D) is not produced and transported as a species but is defined as a fraction of the ALD2 corresponding to an isotope ratio of -86‰, i.e. equal to the isotopic composition of CH<sub>4</sub>.

<sup>b</sup> Discussed in Sect. 2.2.

<sup>c</sup> Here the production of other species than CHDO is neglected because the small amount of ALD2(D), C<sub>2</sub>O<sub>3</sub>(D) OLE(D), ETH(D), or ISOP(D) involved. Actually, the deuterated companion species are not produced or transported but are defined as fractions of the non-deuterated species corresponding to an isotope ratio of -86‰, i.e. equal to the isotopic composition of CH<sub>4</sub>.

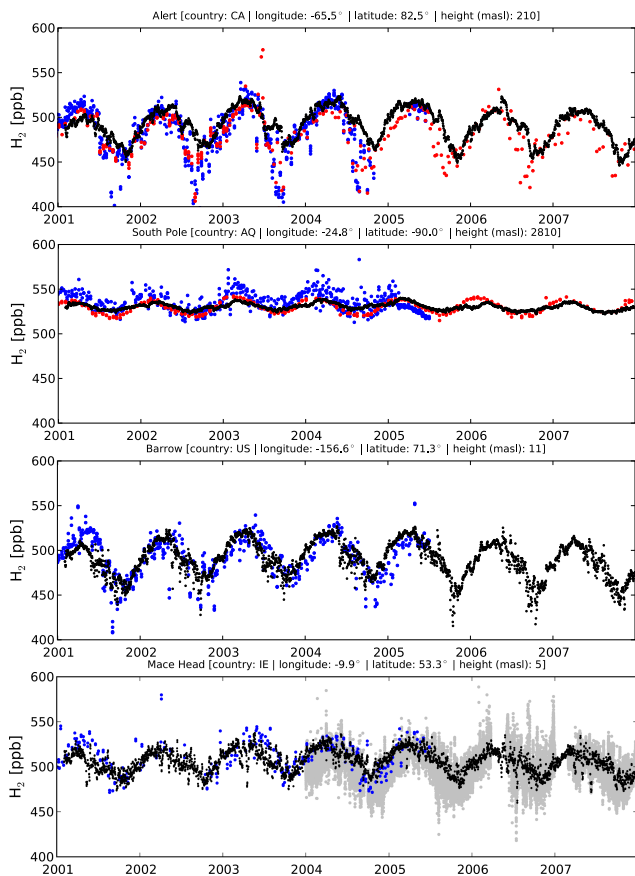


**Fig. 1.** Comparison between the measured background and modelled (black) noon-time  $H_2$  mixing ratios at Alert, the South Pole, Barrow and Mace Head. Available measurements from NOAA, CSIRO and AGAGE are shown in blue, red, and grey, respectively. Measurements from AGAGE are shown without filtering for background conditions.

**Hydrogen isotope modelling**

G. Pieterse et al.

Title Page

Abstract Introduction

Conclusions References

Tables Figures

◀ ▶

◀ ▶

Back Close

Full Screen / Esc

Printer-friendly Version

Interactive Discussion



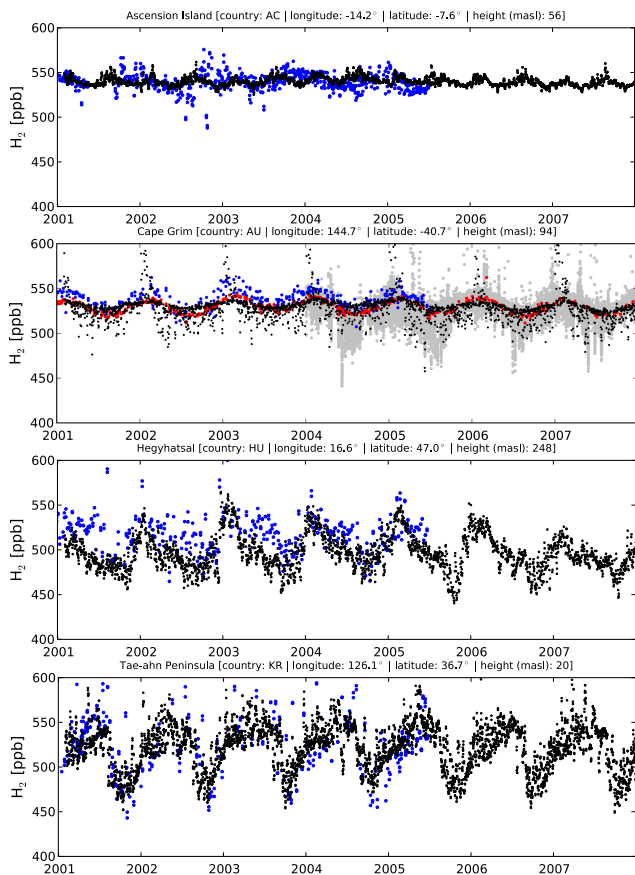


**Fig. 2.** Comparison between the measured and modelled (black) noon-time  $H_2$  mixing ratios at Ascension Island, Cape Grim, Hegyhatsal and the Tae-Ahn peninsula. Available measurements from NOAA, CSIRO and AGAGE are shown in blue, red, and grey, respectively. Measurements from AGAGE are shown without filtering for background conditions.

Title Page

Abstract

Introduction

Conclusions

References

Tables

Figures

◀

▶

◀

▶

Back

Close

Full Screen / Esc

Printer-friendly Version

Interactive Discussion



Hydrogen isotope  
modelling

G. Pieterse et al.

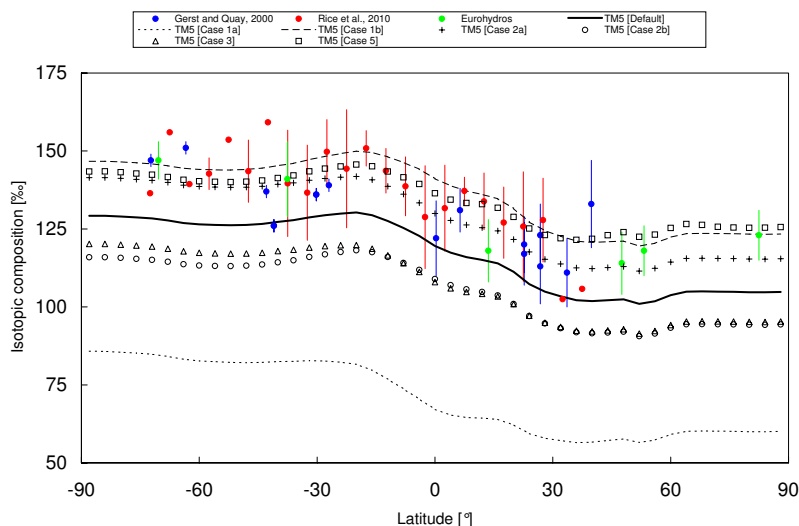


**Fig. 3.** Comparison of the modelled zonal mean surface isotopic composition (thick solid line) with available measurements. Blue circles represent measurements from Gerst and Quay (2000), red circles represent measurements from Rice et al. (2010), and green circles represent measurements from the Eurohydros project (Batenburg et al., 2011). Also shown are some of the cases of the sensitivity study discussed in Sect. 3.6. Case 1a shows the effect of using the KIEs for formaldehyde photolysis as proposed by Feilberg et al. (2007a), case 1b shows the effect of changing the pressure dependency of the molecular photolysis channel for formaldehyde, case 2a shows the effect of increasing the stratospheric isotopic composition by 20‰, case 2b shows the effect of shifting the tropopause pressure level, case 3 shows the effect of decreasing the isotopic composition of the primary NMHCs to  $-200\text{‰}$ , and case 5 shows the effect of reducing the deposition fractionation constant to 0.900.

Title Page

Abstract

Introduction

Conclusions

References

Tables

Figures

◀

▶

◀

▶

Back

Close

Full Screen / Esc

Printer-friendly Version

Interactive Discussion



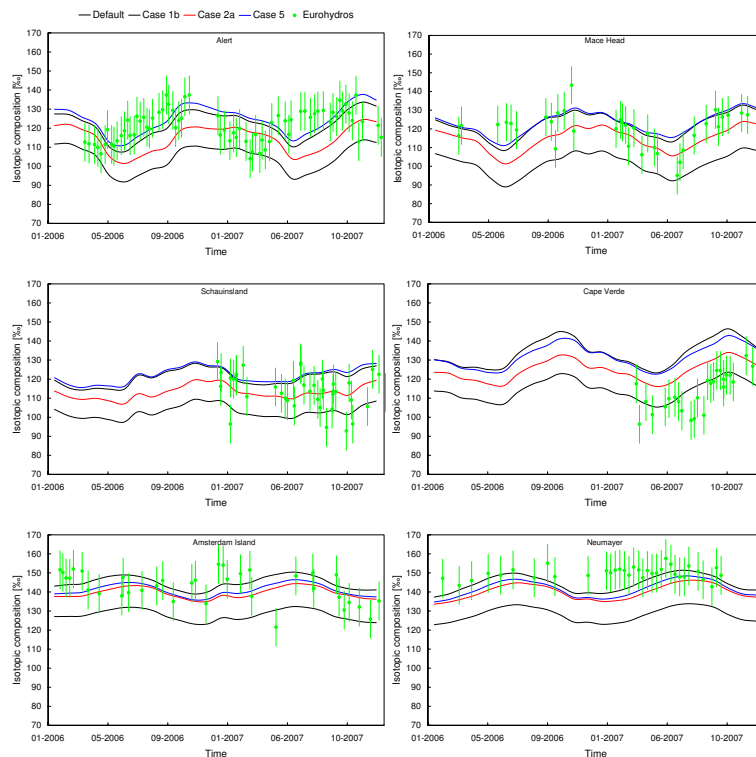


**Fig. 4.** Comparison of the modelled isotopic composition (thick black) with available measurements (green) from Alert, Mace Head, Schauinsland, Cape Verde, Amsterdam Island, and Neumayer. Also shown are some of the cases of the sensitivity study discussed in Sect. 3.6. Case 1b (thin black) shows the effect of changing the pressure dependency of the molecular channel of formaldehyde removal by photolysis, case 2a (red) the effect of increasing the stratospheric isotopic composition by 20%, and case 5 (blue) the effect of changing the deposition fractionation constant to 0.900.

[Title Page](#)[Abstract](#)[Introduction](#)[Conclusions](#)[References](#)[Tables](#)[Figures](#)[◀](#)[▶](#)[◀](#)[▶](#)[Back](#)[Close](#)[Full Screen / Esc](#)[Printer-friendly Version](#)[Interactive Discussion](#)

Hydrogen isotope  
modelling

G. Pieterse et al.

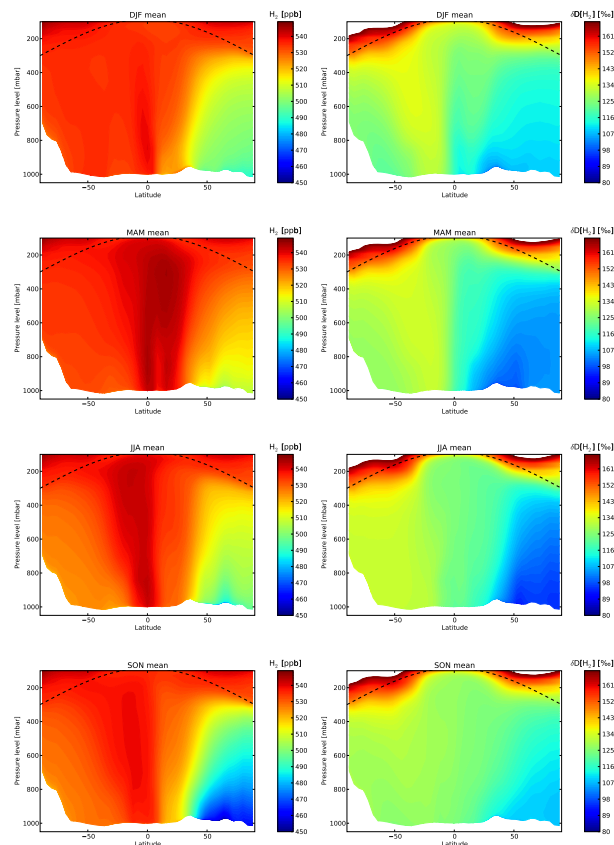


**Fig. 5.** Seasonal zonal mean  $\text{H}_2$  mixing ratio in ppb (left column) and isotopic composition in ‰ (right column) during the NH winter (DJF), spring (MAM), summer (JJA), and autumn (SON) season. The default tropospheric boundary for the stratospheric parametrisation (see Sect. 2.3) is indicated by the dashed line.

Title Page

Abstract

Introduction

Conclusions

References

Tables

Figures

◀

▶

◀

▶

Back

Close

Full Screen / Esc

Printer-friendly Version

Interactive Discussion



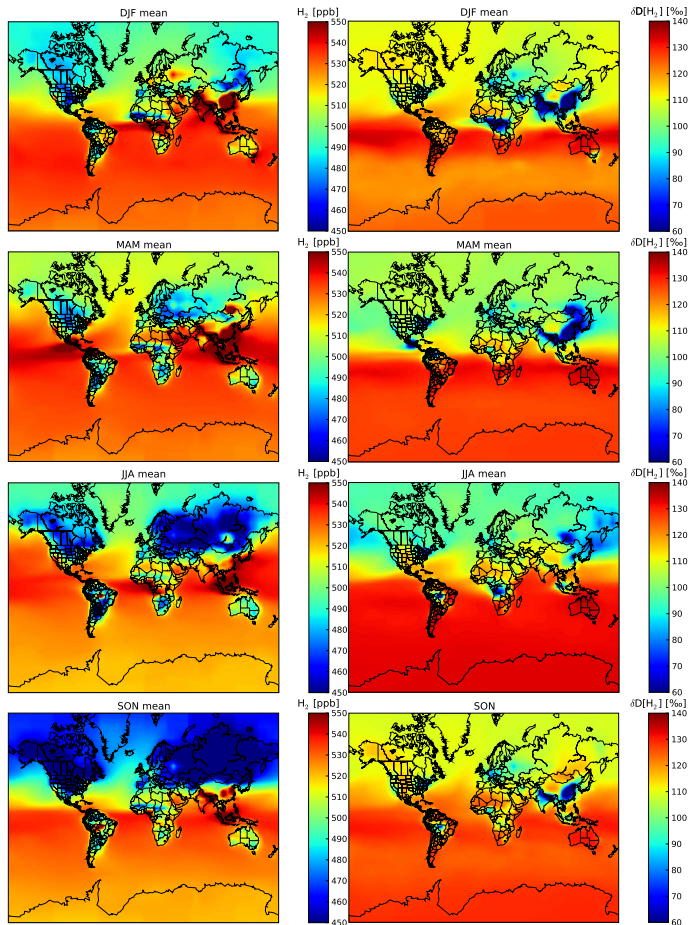


**Fig. 6.** Seasonal mean surface level  $\text{H}_2$  mixing ratio in ppb (left column) and isotopic composition in ‰ (right column) during the NH winter (DJF), spring (MAM), summer (JJA), and autumn (SON) season.

Hydrogen isotope  
modelling

G. Pieterse et al.

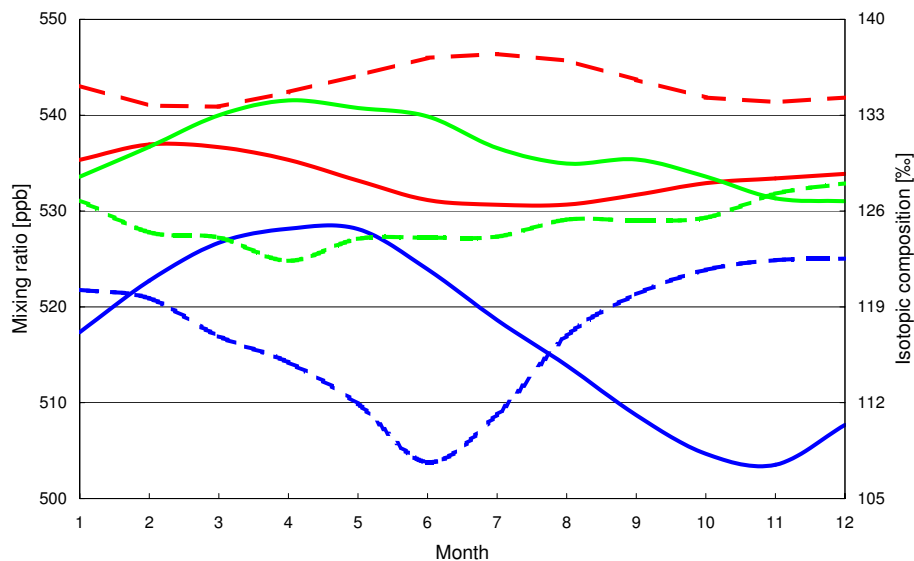


**Fig. 7.** The modelled seasonal cycle of the  $\text{H}_2$  mixing ratio (full lines) and isotopic composition (dashed lines) derived from the budgets of the latitude bands from (blue)  $90^\circ\text{N}$  to  $30^\circ\text{N}$ , (green)  $30^\circ\text{N}$  to  $30^\circ\text{S}$ , and (red)  $30^\circ\text{S}$  to  $90^\circ\text{S}$ .

[Title Page](#)[Abstract](#)[Introduction](#)[Conclusions](#)[References](#)[Tables](#)[Figures](#)[◀](#)[▶](#)[◀](#)[▶](#)[Back](#)[Close](#)[Full Screen / Esc](#)[Printer-friendly Version](#)[Interactive Discussion](#)

## Hydrogen isotope modelling

G. Pieterse et al.

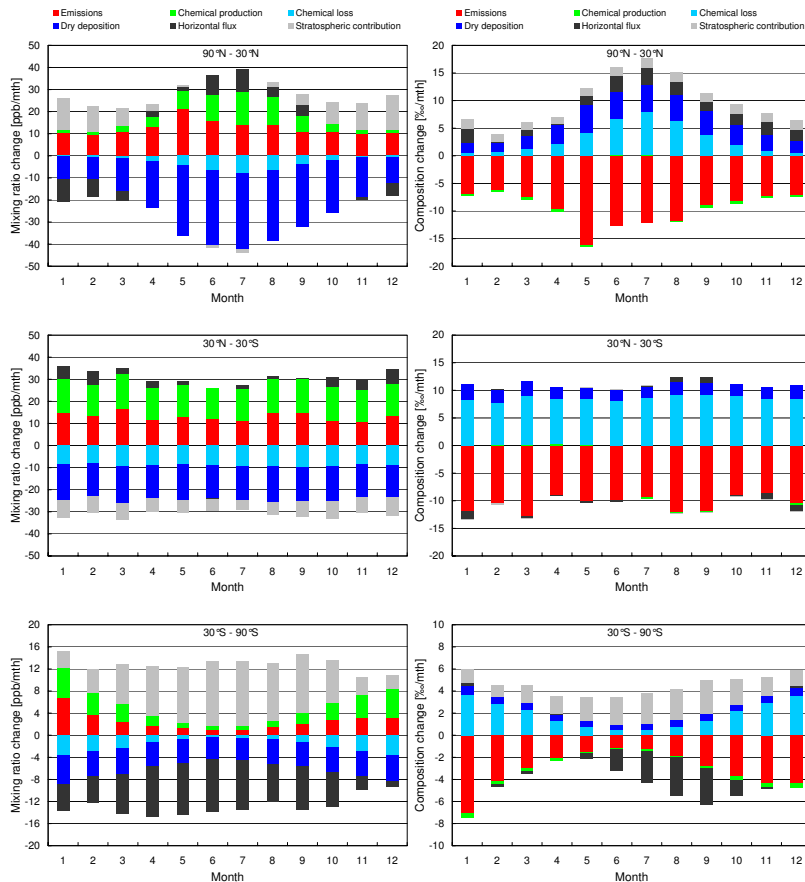


**Fig. 8.** The modelled contributions of the different processes to monthly changes in the mixing ratio (left column) and isotopic composition (right column) in Fig. 7, derived from the budgets of the latitude bands from 90° N to 30° N, 30° N to 30° S, and 30° S to 90° S.

Title Page

Abstract Introduction

Conclusions References

Tables Figures

◀ ▶

◀ ▶

Back Close

Full Screen / Esc

Printer-friendly Version

Interactive Discussion



Hydrogen isotope  
modelling

G. Pieterse et al.

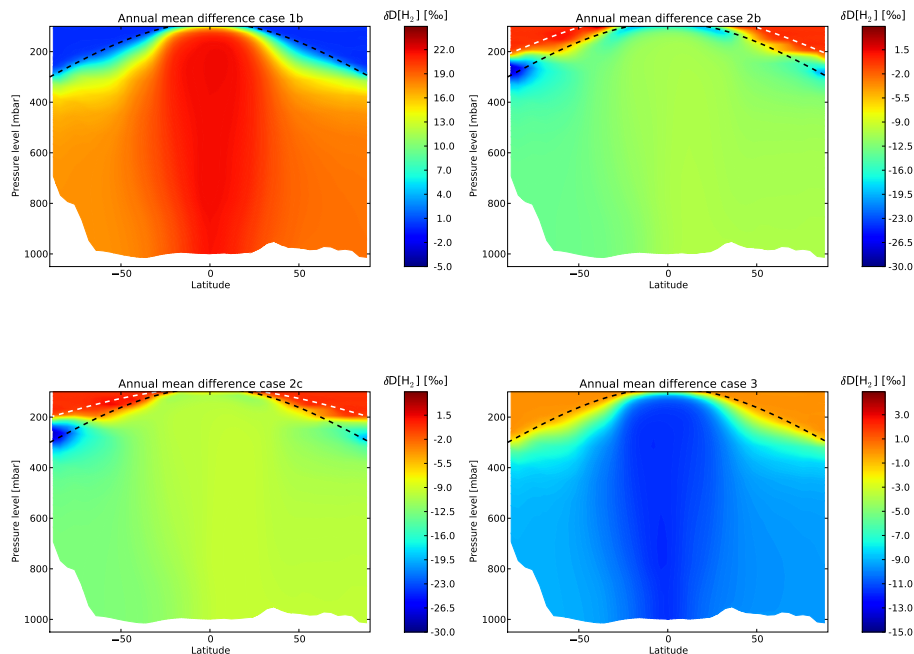


**Fig. 9.** Zonal annual mean differences for case 1b, case 2b, case 2c, and case 3. The default tropospheric boundary for the stratospheric parametrisation (see Sect. 2.3) is indicated by the dashed black line. The perturbed boundaries of case 2b and 2c are indicated by the dashed white line.

Title Page

Abstract

Introduction

Conclusions

References

Tables

Figures

◀

▶

◀

▶

Back

Close

Full Screen / Esc

Printer-friendly Version

Interactive Discussion



Hydrogen isotope  
modelling

G. Pieterse et al.

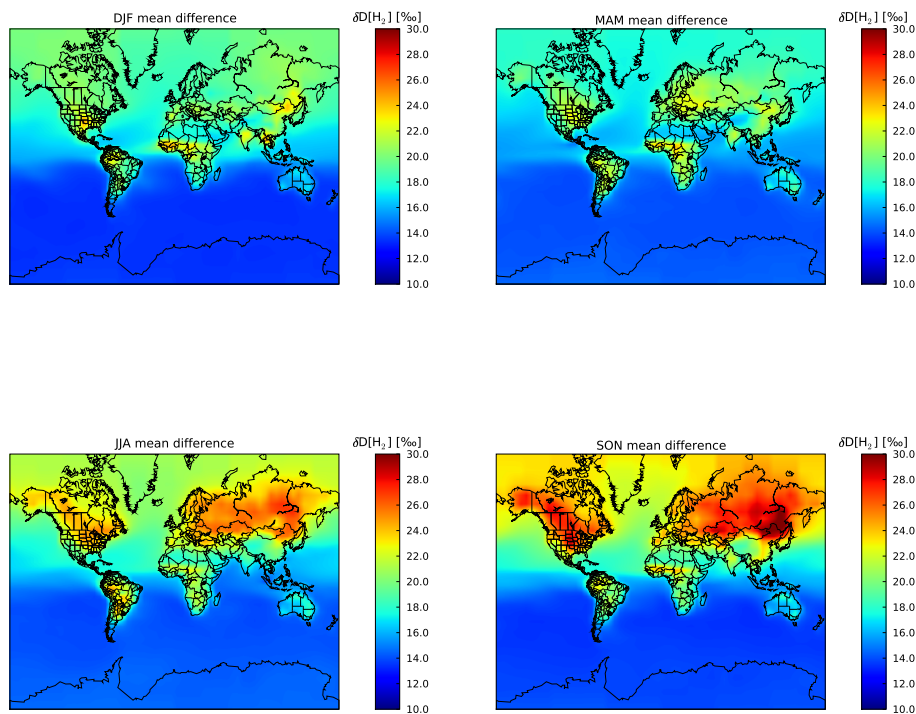
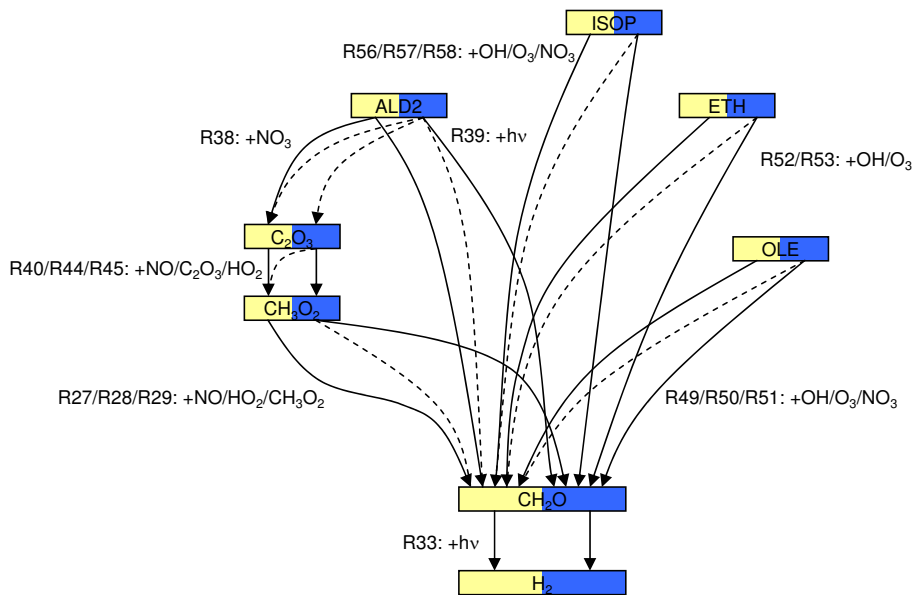


Fig. 10. Case 5 surface level seasonal mean difference.

[Title Page](#)[Abstract](#)[Introduction](#)[Conclusions](#)[References](#)[Tables](#)[Figures](#)[◀](#)[▶](#)[◀](#)[▶](#)[Back](#)[Close](#)[Full Screen / Esc](#)[Printer-friendly Version](#)[Interactive Discussion](#)

Hydrogen isotope modelling

G. Pieterse et al.



**Fig. B1.** NMHC reactions modified for hydrogen isotope chemistry. Yellow container species are non-deuterated, whereas blue container species are singly deuterated species. The solid lines indicate production of the species from the reactant species that is taken into account, whereas the dashed lines indicate production that is neglected (as explained in Sect. 2.2).

Title Page	
Abstract	Introduction
Conclusions	References
Tables	Figures
◀	▶
◀	▶
Back	Close
Full Screen / Esc	
Printer-friendly Version	
Interactive Discussion	

